The Climatic Signal in the Stable Isotope Record of a Shallow Ice Core from NW-Greenland

Hera Guðlaugsdóttir

Jarðvísindadeild
Háskóli Íslands
2013

The Climatic Signal in the Stable Isotope Record of a Shallow Ice Core from NW-Greenland

Hera Guðlaugsdóttir

60 eininga ritgerð sem er hluti af
Magister Scientiarum gráðu í jarðfræði

Leiðbeinandi/endur
Árný Erla Sveinbjörnsdóttir
Hans Christian Steen-Larsen

Prófdómari / Fulltrúi deildar
Þorsteinn Þorsteinsson

Jarðvísindadeild
Verkfræði- og náttúruvísindasvið
Háskóli Íslands
Reykjavík, 4 febrúar 2013

The climatic signal in the stable water isotope record of a shallow ice core from North West Greenland
Stöðugar samsætur voru mældar í grunnum ískjarna fra NV-Grænlandi fyrir tímabilið 1902-2007. Hitastig var metið og borið saman við loftslagsstika. Hafísþekja Baffin Flóa var metin aftur til ársins 1902 með fjölbreytu-aðhvarfsgreiningu.
60 eininga ritgerð sem er hluti af *Magister Scientiarum* gráðu í jarðfræði

Jarðvísindadeild
Verkfræði- og náttúruvísindasvið
Háskóli Íslands
Sturlugötu 7
101 Reykjavík

Sími: 525 4600

Skráningarupplýsingar:
Hera Guðlaugsdóttir, 2013, *The climatic signal in the stable isotope record of a shallow ice core from the NEEM site, NW-Greenland*, meistararitgerð, Jarðvísindadeild, Háskóli Íslands, 62 bls.

Prentun: Háskólaprentun ehf.
Reykjavík, 4 febrúar 2013

Útdráttur

Stöðugar vetnis- og súrefnissamsætur voru mældar úr efstu 39,6 m úr 80 m löngum ískjarna, NEEM S2 08, frá Norð-Vestur Grænlandi. Nákvæm aldursgreining kjarnans sem fyrst og fremst er byggð á talningu 18O árlaga sýndi að mældur hluti hans spannar tímabilið frá 1902 til 2007. Samband milli lofthita og súrefnissamsætna er vel þekkt og í fyrri hluta ritgerðarinnar er meðalárshiti reiknaður og breytingar á honum rannsakaðar. Samsætuferlar voru leiðréttir vegna flakks (e. diffusion) samsætna og árstíðarbundinn munur samsætna og tvívetnisauka rannsakað. Í seinni hluta ritgerðarinnar voru samsætuferlarnir bornir saman við þekkta loftslagsstika af þessu svæði, ásamt hitastigsmælingum frá Stykkishólmi, með því að beita línulegri aðhvarfsgreiningu. Í Baffin Flóa, vestanmegin við Grænlandsstrendur, hafa ísþekjumælingar verið gerðar síðan 1979. Með því að nota samsætuferil súrefnis úr NEEMS208 kjarnanum, ásamt hitastigi Illulisat á V-Grænlandi, var sjávarísþekja Baffin Flóa aftur til ársins 1902 metin með fjölbreytu-aðhvarfsgreiningu. Ferillinn veitir mikilvæga innsýn inn í þann breytileika sem hefur átt sér stað á veðurfari Norðurheimsskautasvæðisins á tuttugustu öldinni.

Abstract

Stable isotopes of hydrogen and oxygen were measured from the uppermost 39.6 m of the 80m NEEM S2 08 shallow ice core from North-West Greenland. The age scale was constructed mainly by counting 18O annual layers, and showed that the analyzed core cover the period 1902-2007. The relationship between air temperature and oxygen isotopes is well known and in the first part of the thesis the mean annual temperature was calculated and changes studied. From the deconvoluted 18O profile, the seasonal signal could be studied, leading to interesting seasonal difference in the isotopic signal and the deuterium excess. In the second part of the thesis the isotopic profiles were compared with known climatic parameters from the area along with Stykkishólmur temperature by using Linear Regression analysis. In Baffin Bay, located to the west off Greenland, ice area measurements have been performed since 1979. By using the NEEMS208 isotopic profile and the temperature from Illulisat, W-Greenland, the sea ice of Baffin Bay could be reconstructed back to the year 1902, or as far back as the isotopic profile goes. That was done by using Multivariable Linear Regression. The reconstructed ice area profile gives an important insight into the climatic changes that have been taking place in the Arctic for most of the 20th century.

Table of contents

List of figures ..... **vii**

List of tables ..... **ix**

Abbreviations & variable names ..... **xi**

Thanks ..... **xiii**

1 Introduction **1**

1.1 Paleoproxies 1

1.2 Overview – Ice core drilling 2

1.3 The NEEM Project 4

2 Geography & climate **7**

2.1 Polar geography and interactions 7

2.2 The North Atlantic Oscillation 9

2.2.1 NAO anomalies 9

2.3 Southern forces 10

3 Stable water isotopes and physical processes in nature **11**

3.1 The δ-scale 11

3.2 Physical properties 11

3.2.1 Physical processes 12

3.2.2 Deuterium excess 13

3.3 Isotopic fractionation 13

3.3.1 Equilibrium fractionations 13

3.4. Diffusion 19

3.4.2. Reversed diffusion 19

4 Sample handling and measurement tecniques **21**

4.1 The IRMS 21

4.1.1 TC/EA 22

4.1.2 Gas Bench 23

4.2 Calibration and precision 24

4.3 The Picarro 25

4.3.1 Technique 25

4.3.2 Measurements and methods 26

4.3.3 Precision 26

4.4 Instrument comparison 28

5 The NEEM 2008 S2 shallow core. Results 29
5.1 The isotopic data set 29
5.2 The age scale 31
5.3 Temperature reconstruction 34
5.4 Annual and seasonal signal 36
5.5 Natural variability: The comparison between NEEMS308 & NEEMS208. 41
5.6 Summary and discussions 43
6 Comparison between the isotopic signal of NEEM S2 2008 shallow core and climatic parameters 45
6.1 Iceland and climatic parameters 46
6.1.1 Results 46
6.2 Greenland and climatic parameters 46
6.2.1 Results 46
3.5. Baffin Bay Sea Ice reconstruction 47
6.2.2 Results 48
6.3 Summary and discussions 50
7 Discussions 53
8 Conclusions 55
References: 57

List of figures

Figure 1-1: δ18O data from five of the deep ice cores, all spanning an interval of 120 thousand years and Renland, a shallow (324m) ice core drilled through the Renland ice cap (Johnsen et al., 2001). 3

Figure 1-2: Isotope data for NGRIP & GRIP (δ18O) and Vostok & EPICA Dome C (δH) (Petit., et al. 2001, Jouzel., et al. 2004, Center for Ice and Climate, 2006). The end of the warm Eemian period in Greenland is observed in the decline around 120.000 years BP. 4

Figure 1-3: The main deep drilling sites and the NEEM site. 5

Figure 2-1: The polar ice sheets and their geography (Exploratorium, 2013). 7

Figure 2-2: The arctic circled by the green area. Baffin Bay lies west of the Greenland coast. 8

Figure 2-3: The high (H) and low (L) pressure zone of the NAO and the area affected (OSS, 2013). 9

Figure 3-1: An example of the seasonal 18O signal observed in a GRIP pit core spanning 4 years. It´s correlation with temperature is also shown (Vinther, 2006). 12

Figure 3-2: A schematic figure of the surface and boundary layers. 14

Figure 4-1: The inside of the IRMS here shown along with the mass-dependent path from the ion chamber to the output signal (U.S Geological Survey, 2013). 21

Figure 4-2: TC/EA inlet and the path the sample takes before entering the IRMS. 22

Figure 4-3: A schematic picture of the sample path in the Gas Bench along with the output signal as shown on screen (in mV). 24

Figure 4-4: CRDS system and the Ring down (Picarro, 2012). 25

Figure 4-5: Difference between the Ring-down timing with and without sample (Picarro, 2012). 26

Figure 5-1: The linear relationship of δD and $\delta^{18}O$ of the NEEM 2008 S2 shallow core. 29

Figure 5-2: $\delta^{18}O$ (gray), δD (black) and the d excess (green) plotted on a depth scale. There are still some outliers that need to be re-measured. They are most obvious in the d excess profile. 30

Figure 5-3: The raw and deconvoluted profile (blue and gray) $\delta^{18}O$ profile. The red lines indicate fixed points used. 32

Figure 5-4: The $\delta^{18}O$, raw (blue) and deconvoluted (gray) profiles constructed on an age scale. 33

Figure 5-5: The isotopic temperature profiles of the deconvoluted (grey) and the raw (blue) data. 35

Figure 5-6: Between the dotted lines is the annual isotopic layer of 1987 occurring between 10 and 11 m depth in the NEEMS208 shallow core. For clarification red arrows point at summer peaks and black arrows to winter peaks. 36

Figure 5-7: Mean annual isotopic profile from 1902-2007. The cold decades between 1920 and 1940 are also observed with the 20 year cycle repeating until 1984. After that is a clear trend. When the temperature is studied between 1980 and 2007, the average temperature rise is 0.093°C per year in the NEEM area, equivalent to 2.5°C rise for the æast 27 years. 38

Figure 5-8: The seasonal temperature profile using only the heaviest values as summer and lightest as winters. The difference between trends for summer (green) and winter (blue) can be seen along with the increasing difference after 1960. The gradual temperature change appears to begin after 1980. The trend for the average summer and winter temperature is 0.2°C and -0.15°C per year, respectively, from 1980 to 2007. 39

Figure 5-9: A comparison between the d excess (green) and the $\delta^{18}O$ (black) profiles. The difference in the seasonal signal between profiles displays a lag of 2-3 months. 40

Figure 5-10: A comparison between the NEEM08S2 and NEEM08S3 shallow core. The good correlation is quite visible between S3 (blue) and S2 (black) although there are differences, f. Ex. Between 1910 and 1914. 42

Figure 5-11: Annual global mean temperature anomaly. The green bars represent uncertainty estimations. (Hansen et al., 2001). 43

Figure 5-12: Total solar irradiation (Green) (Laboratory for Atmospheric and Space Physics, 2013) compared to the mean annual $\delta^{18}O$ signal (black). The dotted lines are given to facilitate a comparison between the two records. 44

Figure 6-1: Geographic location of the Baffin Bay. 47

Figure 6-2: The correlation if only $\delta^{18}O$ is used to reconstruct the BBSIA is R = 0.06. 48

Figure 6-3: Measured (red) and calculated (blue) BBSIA profiles from 1979 to 2007 49

Figure 6-4: Calculated BBSIA from 1902 to 2007. 49

Figure 6-5: Comparison of the climatic parameters studied in chapter 6. They are Stykkishólmur and Illulisat T (°C) (black), reconstructed BBSIA (km^2) for the 20th century (dashed) along with the measured profile (red), the annual $\delta^{18}O$ profile (green) and the annual NAO index (blue). 51

List of tables

Table 1-1: Deep Greenland ice cores 2

Table 4-1: The changes of residuals with time and length. Not all runs had test samples and the run length varied, explaining the emty rows and seats. 27

Table 4-2: Results showing the same samples measured for $\delta^{18}O$ in the GB and the Picarro and for δD in the TC/EA and the Picarro and the resulting difference between instruments. 28

Table 6-1: Estimate on correlation based on R..... 45

Table 6-2: The Correlation (R) between Stykkishólmur T and NAO, annual $\delta^{18}O$ and Illulisat T..... 46

Table 6-4: Correlation (R) between several different climatic parameters over specified time intervals given in parentheses. 47

Abbreviations & variable names

NEEM = North Eemian project

NH = North Hemisphere

NAO = North Atlantic Oscillation

NADW = North Atlantic Deep Water

ITCZ = Inter Tropical Convergent Zone

SMOW = Standard Mean Ocean Water

IRMS = Isotope Ratio Mass Spectrometer

TC/EA = High Temperature Elemental Analyzer

CRDS = Cavity Ring Down Spectroscopy

BBSIA = Baffin Bay Sea Ice Area

BBSIE = Baffin Bay Sea Ice Extent

LR = Linear Regression

MLR = Multivariable Linear Regression

δ = scaled isotopic value

R = ratio between the concentration of heavy and light isotopes

‰ = promil, parts per thousand

T = temperature

h = Relative Humidity (RH)

d = deuterium excess

α = fractionation factor

J = molecular flow

D = diffusivity

dN_E = net flux of evaporation

dN_P = net flux of precipitation

E = net flow

ρ = density

z = height

q = specific humidity

q_s = saturated specific humidity

Γ = the profile coefficient at z

u_0 = friction velocity

ρ_M = molecular resistance

ρ_T = turbulent resistance

F = surface flow

D = diffusivity in air

e_v = partial pressure

e_i = saturation vapor pressure over ice

C_{smow} = isotopic ratio of the SMOW

n = particle density

∇^2 = laplacian operator

k_b = Boltzman constant

v_n = mean velocity

l_n = mean free path

γ = damping factor

τ = mean time between collision

l = distance

m = mass

μ = mobility

c = constant

v = volume

λ = wavelength

k = wave number

L = diffusion length

F_1 = symmetrical filter

$\overline{F_1}$ = Fourier transform of F_1

ε_i = noise

Thanks

I want to thank the following: RANNÍS for funding this project, the Icelandic Meteorological Office for Stykkishólmur temperature data support, Rósa Ólafsdóttir for measurement, teqnical assistance and more, Þorsteinn Jónsson also for teqnical assistance, my father Guðlaugur Kristinn Óttarsson for enhancing concepts and instructive discussions, Birna Geirfinnsdóttir for graphical assistance and Geirfinnur Svavarsson for housing me at Húsavík while working on this project, Katla Rós Völudóttir for graphical assistance, and the office girls for being wonderful.

My family, Jón Ragnar, Ísleifur and Flóki, deserves special thanks for patience, love and support along with my mother, Valborg Kristjánsdóttir and Vilborg Jónsdóttir and Daði Hilmar Ragnarsson.

I would also like to thank Sigfús J. Johnsen, my third supervisor, for giving me insight into his theory and high spirited mind. Last but not least I would like to thank my supervisors: Árnýju Erlu Sveinbjörnsdóttur for trusting me with this project and for inspiring and fruitful guidance and support and Hans Christian Steen-Larsen for deconvoluting the data and for putting the pieces togeather.

1 Introduction

In recent years and decades climate change has been a subject of many debates. The anthropogenic influence is now thought to be the main cause, as reflected in the fast rise in the concentration of carbon dioxide (CO_2). Still voices are heard disagreeing on the cause but the fact remains that climate is changing. Prior to 1850 the atmospheric concentration has risen from 278 parts per million (ppm) to 394ppm in 2012 (Earth System Research Laboratory, 2012). The role of other factors is also studied, such as changes in insolation of the Sun and volcanic eruptions (Hansen & Lacis, 1990) (Robock, 2000), methane production of live stock and microbes (Hansen et al., 2000) along with natural fluctuation.

1.1 Paleoproxies

In order to understand the present climate and the controlling forces climate proxies for past environment is of utmost importance. Monitored climatic parameters are of course too of great value when tracking present climatic changes. That is specially the case if those parameters are continuous over a long period of time. An example is the CO_2 measurements on Mauna Loa since 1958 and the temperature measurements that have been done in Stykkishólmur, Iceland, since the 19th century. However, the instrumental records are limited as they only cover changes during the last century or so. When the focus is on paleoclimate and the future climate evolution, a comparison with the pre-historic past is of great value. Information will then be put into a right perspective where changes in trends and rates will be more informative. In order to do so, different climate proxies are needed. The physical nature of isotopes makes them highly suitable to retrieve information on the past. One of the best archives on paleoclimate exists on the poles where snow has settled, layer upon layer for hundreds of thousands of years. There, summer melting has not affected the vast archives that can be found within the ice and thus part of Earth´s history can truly be read from there. For example, information on ancient temperature from stable water isotopes (Dansgaard, 1953), atmospheric compositions from enclosed gas bubbles (Oeschger et al., 1984) and wind directions, solar insolation and volcanic eruptions from dust in the ice (Petit et al., 1981, Oeschger et al., 1984). The rapid melting of the Greenland ice sheet in recent years has raised concerns about its future. A race with time has begun and the need to retrieve the climatic history of the Northern Hemisphere will increase in the coming years.

The oldest ice close to bedrock at the GRIP site (see sub-chapter 1.3. for details) in Greenland is thought to be around 250.000 years old (Souchez, 1997). Despite that, reliable, high resolution climatic information has only been retrieved so far from the Greenland ice sheet for the last 123 thousand years (NGRIP members, 2004). For comparison, the Antarctic ice sheet gives information on climate that spans at least 800 thousand years (Luthi et al., 2008). The study of these ice sheets has brought focus to the ocean-atmospheric dynamics between the two hemispheres and how that is displayed in a seesaw-like pattern (Steig et al., 1998). In that millennial-scale context, interesting oscillations are revealed in polar ice cores. Those oscillations, or cycles, are related to Earth´s rotation and its orbit around the Sun, referred to as the Milankovich cycles. They occur on 100.000, 41.000 and 21.000 year intervals and refer to the cycles of Earth´s

eccentricity, obliquity and precision respectively. Their importance can be described as a pacemaker for glacial and interglacial periods (Hays et al., 1976), although their exact influence on climate is still of some debate.

As can be seen from this short overview above, much of our understanding on past Earth´s climate and it´s behavior comes from information retrieved from polar ice cores even though ice core studies have only been conducted for about half a century or so. In this thesis the main focus is on the isotopic depth profiles retrieved from the 2008 S2 shallow core from the NEEM site, North West Greenland. From the isotopic profile the temperature is constructed and studied. The climatic parameters that govern the area of interest are also studied and compared to the isotopic profiles.

1.2 Overview – Ice core drilling

The first to discover the use of isotopes in paleoclimatology was Harold Urey, a chemist who received the Nobel Prize for discovering the heavy hydrogen in 1934. He discovered the relation between the isotopic fractionation factor and temperature when studying isotopic oxygen fractionation in calcium carbonate (Urey, 1947). Dansgaard discovered the isotopic signal in precipitation and it´s relation to temperature at the site of formation (Dansgaard, 1953), influencing this field of science for years to come. When the Camp Century deep ice core was drilled in Greenland in 1962-1966 the seasonal signal was revealed in the ice along with 100.000 years of temperature data (Dansgaard et al., 1969). Since Camp Century, five deep ice cores have been drilled in Greenland (see table 1.1).

Table 1-1: Deep Greenland ice cores

Site	Year	Depth (m)
Camp Century	1962-1966	1390
Dye 3	1979-1981	2037
GRIP	1989-1992	3029
GISP2 (US)	1989-1993	3053
NGRIP	1997-2003	3085
NEEM	2007-2010	2537

When searching for the right site to drill, several things must be kept in mind. The ice flow should be simple or none like on the ice divide and the bedrock should be flat for the stratigraphy to remain undisturbed (Dansgaard et al., 1993). Surface melting should be none to minimize changes in the original chemical composition of the precipitation. At certain places, especially in Northern Greenland, geothermal melting occurs at the bottom resulting in loss of the oldest ice. Nowadays radar sounding images have been used when choosing a drill site which can detect basal melting along with other important glaciological information (Dahl-Jensen et al., 2003).

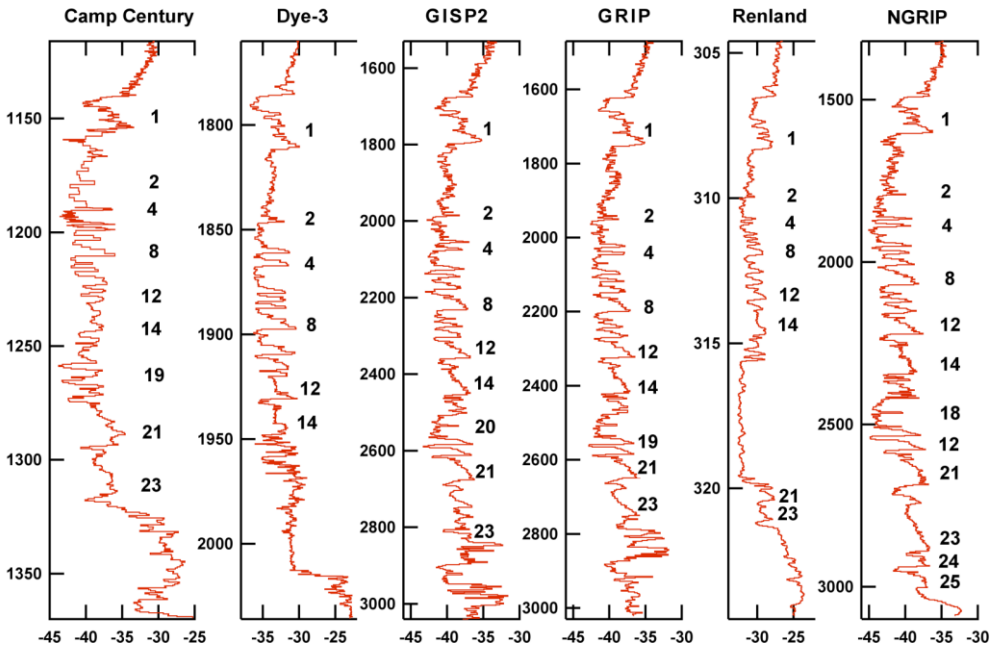

Figure 1-1: δ18O data from five of the deep ice cores, all spanning an interval of 120 thousand years and Renland, a shallow (324m) ice core drilled through the Renland ice cap (Johnsen et al., 2001).

In the timeperiod from 1960´s to 1980´s the first two deep ice cores from Greenland, Camp Century & Dye 3 along with deep cores from Antarctica (Byrd Station, Vostok and Dome C) improved greatly the understanding of paleoclimate and it´s behaviour globally. They showed unexpected rapid climate changes during glaciation but the scientific community was in doubt. When GRIP and GISP2 were drilled on the ice divide at Summit during the years 1989-1993 both the drilling and analytical techniques had improved. The cores gave high-resolution data into the last glaciation, confirming earlier findings of dramatic climate changes during the last glaciation (Johnsen et al., 1997). The cores were 30km appart and spanned an interval of 120 thousand years. The isotopic measurements showed good agreement for the first 90% of the isotopic profiles, representing 110 thousand years, as can be seen in fig. 1.1. The figure also demonstates the good agreement with the Camp Century, Dye-3, Renland and NGRIP cores. The dating of the cores was mostly done by counting the annual layers, but deeper in the cores a steady state ice flow model was used to help construct the chronology (Dansgaard et al., 1969). The coherency between the cores erased any doubt that the isotopic oscillations observed in the Greenland ice cores are of climatic origin. Despite the success, the stratigraphy in the bottom layers of GRIP and GISP2 differed due to disturbed flow at bedrock. Thus a different site had to be found that had the bottom layers intact (Dowdeswell & White, 1995). The drilling of NGRIP on the ice divide some 110 km NW of Summit (figure 1.3) finished in 2003. The purpose being to retrieve the deepest Greenland ice, including ice from the Eemian.

The Eemian was an interglacial period 130-115ky before present (BP). Earlier findings had suggested a relatively stable climate which was 3-5°C warmer than present. Thus, by studying the warm Eemian ice valuable information about the present global warming predictions could be revealed.

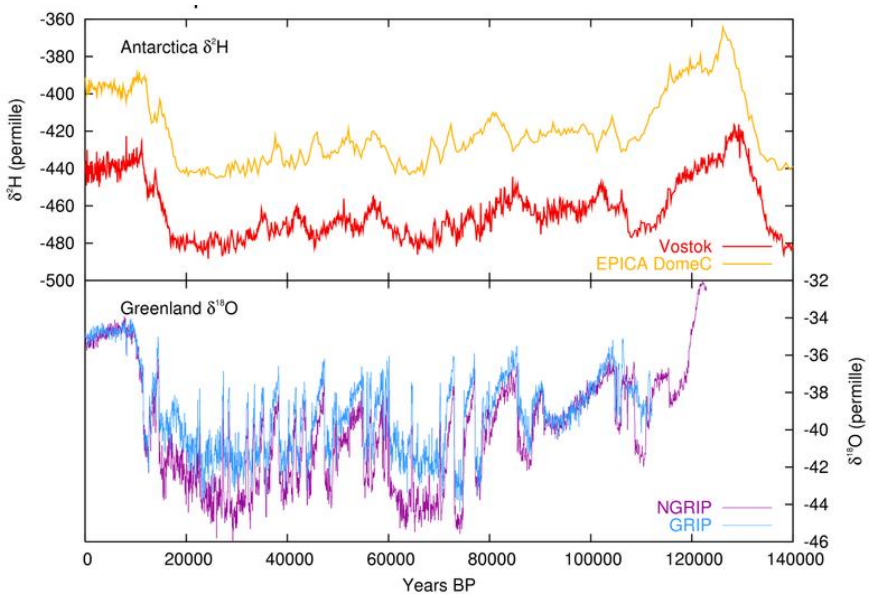

Figure 1-2: Isotope data for NGRIP & GRIP (δ18O) and Vostok & EPICA Dome C (δH) (Petit., et al. 2001, Jouzel., et al. 2004, Center for Ice and Climate, 2006). The end of the warm Eemian period in Greenland is observed in the decline around 120.000 years BP.

The NGRIP ice core revealed important information on the climate behavior during Holocene and the last glaciation due to its exceptionally high resolution (Andersen & al., 2006). It also gave an insight into the end of the Eemian period (fig. 1.2), both in the North and South hemispheres, but the bottom layers had disappeared due to melting (NGRIP members, 2004). In 2007 the North Eemian (NEEM) project started, drilling the NEEM ice core, the second attempt in trying to get the Eemian period undisturbed.

1.3 The NEEM Project

The NEEM deep drilling site is located on the ice divide in the northwestern part of Greenland (77.5N, 50.9W), see fig. 1.3. There, the ice is 2542m thick with an annual ice accumulation of 0,23m. When choosing a site it is important that the accumulation is not too large in order to prevent the ice from flowing and if too little, the seasonal signal could be missed. On the ice divide the problem of ice flow due to weight is mostly avoided though. As mentioned before, the aim of the NEEM deep ice core is to retrieve the Eemian period intact and also to get a complete chronology with high resolution climate profile for the past 140kY BP. In order to do so, shallow reference cores are needed. Three shallow firn/ice cores, NEEM 07 S1, NEEM 08 S2 and NEEM 08 S3, were drilled in 2007 and 2008 with the NEEM 08 S2 core being the subject of this thesis. The main purposes of the shallow ice cores are to:

I. Facilitate dating of the deep ice core and to calculate the signal-to-noise ratio at the site.
II. Obtain a detailed temperature profile for the last 3-400 years.
III. To study the climatic signals in the ice and the forces behind them in order to get a better understanding of the present climate changes we are faced with.

In this thesis only part of the above mentioned objectives are discussed. The signal-to noise ratio calculations are not possible with only one shallow core and are therefore beyond the scope of this study. A detailed temperature profile is obtained for the last 105 years and consequently, the climatic signal covers the same period.

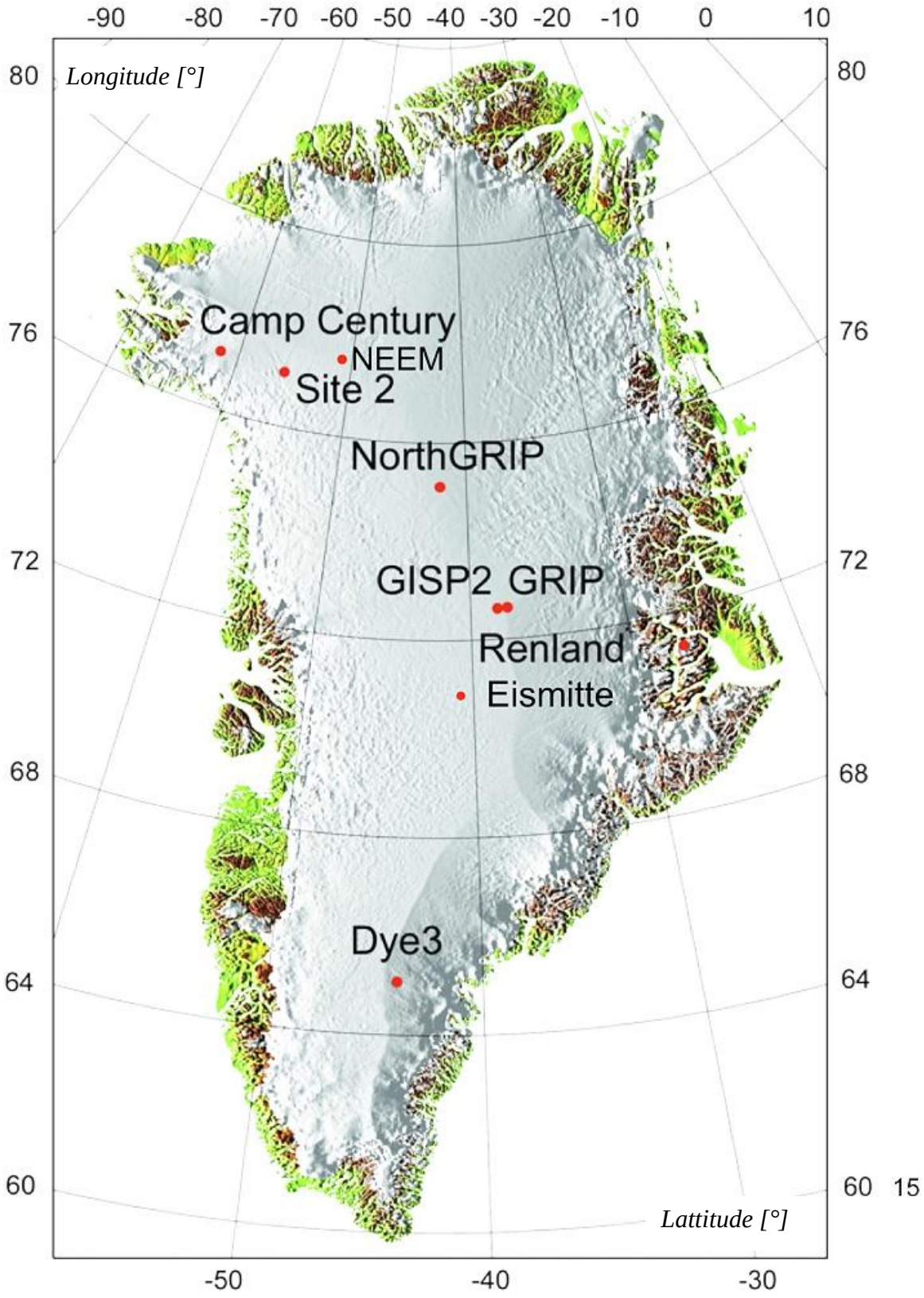

Figure 1-3: The main deep drilling sites and the NEEM site.

2 Geography & climate

Long-term variations in the North Hemispheric (NH) climate leave a clear mark on the mid- and South-Greenland ice sheet. This chapter is an overview on the geography and the climatic parameters influencing (directly or indirectly) the precipitation falling on the Greenland ice sheet. Also, the moisture transport will be discussed.

2.1 Polar geography and interactions

The Greenland ice sheet along with the Arctic area is more vulnerable to climate than the Antarctic ice sheet. The difference in the geographic settings can be seen in fig. 2.1. One of the characteristics of the NH is the landmass which is located there. Complex weather systems govern this part of Earth due to ocean-atmosphere-land interactions. Surface winds, along with Ocean density difference, take part in forcing the Ocean´s Convective belt, including the Gulf Stream, towards the north, providing warmer sub-tropical air to N-Europe. In the Norwegian Sea and Labrador Sea, the warm surface ocean cools and sinks to form North Atlantic Deep Water (NADW) (the main drive of the Convective belt, also called thermohaline circulation) where it get´s transported south to Antarctica (Rahmstorf, 1996). Antarctica is protected by the vast ocean and the Antarctic circumpolar current, also controlled partly by surface winds. The same ocean/wind system then controls the sea ice extent, either holding the ice in a restricted place or allowing the ice to spread (White & Peterson, 1996). The cooling of the NH has been shown to result in a warming of the SH and vice versa, due to changes in the NADW. This response, referred to as the Seesaw effect, has been confirmed by the deep Antarctic ice cores Byrd and Vostok (Crowley, 1992).

Precipitation is very little far up on the Antarctic ice sheet so usually the ice is better suited for an average temperature profile for hundreds of thousands of years instead of a seasonal profile like the Vostok site. An exemption is the EPICA Dome C deep core, drilled on Dronning Maud Land. There, precipitation is high enough to show seasonal signal in the ice.

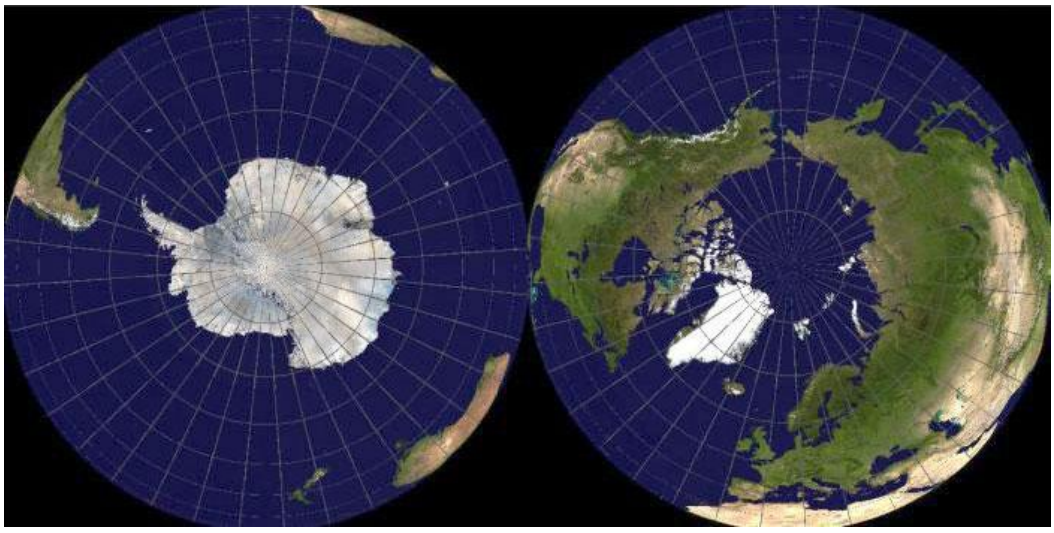

Figure 2-1: The polar ice sheets and their geography (Exploratorium, 2013).

The Arctic area consists of the Arctic Ocean, part of Canada, Alaska, Russia, Finland, Denmark (Greenland), Norway, Sweden and Iceland (see fig. 2.2). The rapid decline in Arctic sea ice has raised anthropogenic and climatic concerns about its future and the global effect. It is thus interesting to see if the stable water isotopes of the NEEM 2008 S2 shallow core record these changes. In Baffin Bay, located to the west of the Greenland coast, sea ice measurements exist from 1979. They have been studied and compared to other parameters, f.ex. a shallow NEEM core drilled in 2007 (Steen-Larsen et al., 2011). Temperature measurements on the west coast of Greenland have been conducted for many decades. For example, llulisat temperature measurements exist from the year 1873 and in Upernavik from 1881. Temperature in the east coast is not as well recorded, the longest one being from 1894 in Ammasalik. Since good correlation was found between Ammasalik and Stykkishólmur (Iceland) temperature, the latter one has been used in previous Greenland ice core studies (Vinther et al., 2010). Stykkishólmur temperature measurements, conducted from the year 1846, will be used in this thesis.

In light of the above-mentioned meteorological data, a comparison between several different meteorological proxies can hence be made on the NEEM S2 2008 shallow core. Climatic signals from several isotopic profiles from SW- and mid-Greenland have been well studied along with one NEEM shallow core drilled in 2007. It will thus be interesting to compare known results to ones presented in this thesis.

Figure 2-2: The arctic circled by the green area. Baffin Bay lies west of the Greenland coast.

2.2 The North Atlantic Oscillation

The North Atlantic Oscillation (NAO) is the main forcing in the NH climate. NAO is thus of special interest and will be analyzed and compared to the isotope record in order to better understand which climatic parameters are affecting north-west Greenland. NAO is driven by pressure oscillations between Iceland and the Azores. When in positive mode, the pressure difference is large and thus strengthens the westerly winds across the Atlantic Ocean (Ahrens, 2009). That directs strong storms into northern Europe and eastern US where winters tend to be wet and mild but northern Canada and Greenland are usually cold and dry, see fig. 2.3. The pressure difference decreases when in negative mode and thus decreasing the westerlies, moving fewer and milder storms more westwards, in turn leaving winters in northern Europe cold and dry. This climatic phenomenon is sometimes refered to as the NAO temperature seesaw pattern (van Loon & Rogers, 1978).

2.2.1 NAO anomalies

Winters in South- and mid-Greenland are specially affected by the NAO as recorded in stable water isotoped (Rogers et al., 1998, Appenzeller et al., 1998). Although the NAO is considered to be quite stable, 20-30% of the winter temperature show a non-seesaw pattern (Vinther et al., 2003). The authors studied the only known breakdown in 135 years of the NAO winter temperature seesaw in Jan-Feb of 1984. They noticed unusual winter temperatures both in Greenland and the British Isles, not a normal pattern for the NAO. When compared to a normal NAO winter in 1989, it was concluded that the 1984 abnormal conditions were associated with a difference in the direction of cyclone tracks.

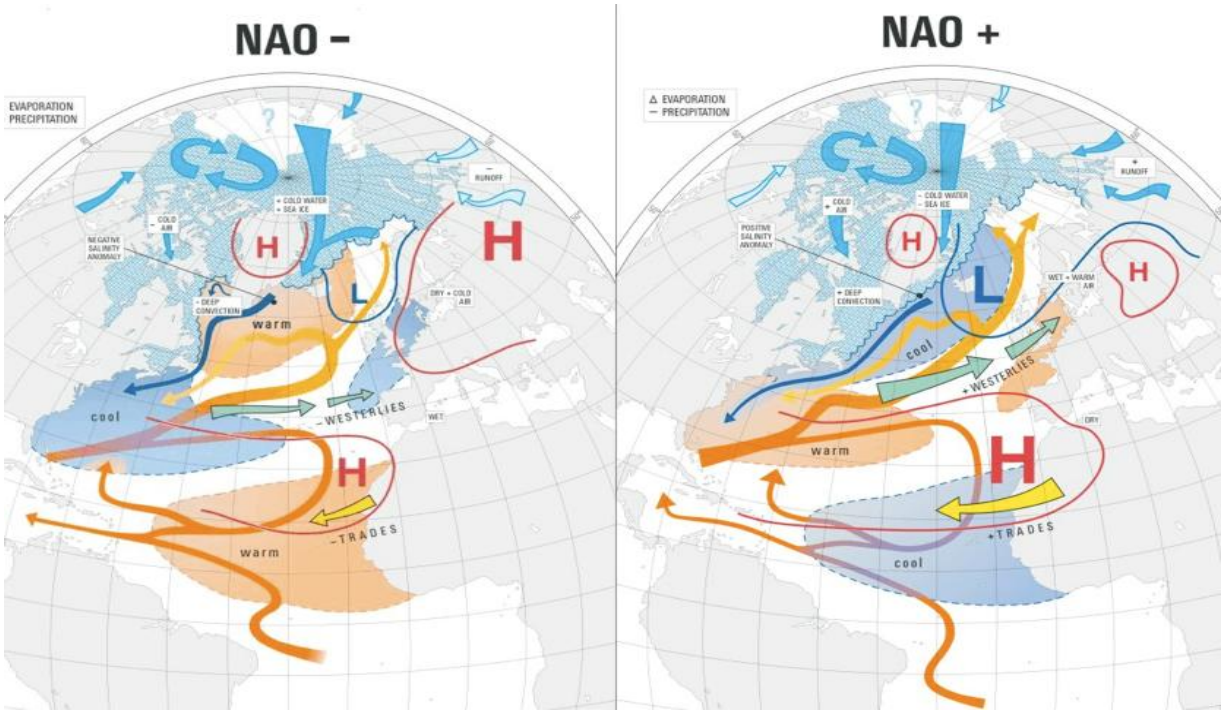

Figure 2-3: The high (H) and low (L) pressure zone of the NAO and the area affected (OSS, 2013).

2.3 Southern forces

The forces that affect the Arctic from the South play an important role, both directly and indirectly.

The Hadley cell

The atmospheric vapor transport is controlled by a conducting atmospheric cell called the Hadley cell. It is a thermal loop, driven by the energy of the sun as warm air rises and cold air sinks (Ahrens 2009). In a simple model it is the only cell that drives winds towards the poles, however the Earth´s rotation must also be taken into account. The energy that the equator (at 0° latitude) receives from the sun results in extensive evaporation in that area. The evaporation is transported upwards with the warm sub-tropical air via the Hadley cell, where it is moved horizontally along the tropopause. When arriving at the 30° latitude the air starts to sink, forming high pressure area. Some of the air goes back to the equator but part of it travels towards the poles via the westerlies in a loop called the Ferrel cell. This division of air is due to the rotation of the Earth, or the Coriolis effect. At the 60° latitude air starts to rise, resulting in a low pressure area, and form what is referred to as the polar front. A cyclonic system then condenses there to form precipitation and according to (Johnsen et al. 1989), most of the precipitation in Greenland comes from cyclones at the polar front.

ENSO

Similar to the NAO is the South Oscillation (SO), also referred to as the El Nino Southern Oscillation (ENSO), positioned on the equator. Atmospheric pressure oscillates due to westerly trade winds between in the eastern and western part of the Pacific Ocean resulting in a seesaw pattern (Bjerknes, 1969). El Nino describes the abnormal situation when the atmospheric pressure decreases in the east, above the coast of South America, and rises in the west, above the coast of Indonesia. The normal condition is referred to as La Nina with higher pressure in the east than in the west. This pressure difference affects the thermohaline circulation in the pacific, a subject irrelevant to this context. Strong ENSO events can affect the NAO and thus the temperature in the north hemisphere (Brönnimann et al., 2007).

ITCZ

Inter-tropical Convergent Zone (ITCZ) is a boundary where the Northeast trade wind converges with the south east trade winds along the equator. A relationship between ITCZ and climate at higher latitudes has been confirmed. In a study from 2006, a model was used indicating that a southward displacement of ITCZ resulted in a cooling in the northern hemisphere (Broccoli et al., 2006). When the ITCZ shifts north, it then results in a warming. In another study from (2008 the last two abrupt warming at the onset of our present interglacial period were studied. There it was proposed that the 2-4K changes in the moisture source between years were the result of the northward displacement of the ITCZ (Steffensen et al., 2008).

3 Stable water isotopes and physical processes in nature

Due to physical characteristics of isotopes, changes through time are securely recorded - regardless of the sample type and the isotopic species involved. There are two types of isotopes that record changes by different routes, they are:

I. Radioactive isotopes. Isotopes with unstable decaying nucleus.
II. Stable isotopes. Isotopes with stable, non-radioactive nucleus.

The type of interest here are the stable isotopes, namely stable water isotopes. In nature, water (H_2O) has several different chemical compositions depending on the weight of the atoms involved. The oxygen stable isotope species have masses 16, 17 and 18, and hydrogen has 1 and 2 (hydrogen with mass 2 is referred to as Deuterium, or D, from now on). These five hydrogen and oxygen isotopes mixes in nature to make nine different water molecules, but the three most important molecules are $^1H_2{}^{16}O$, $^1H_2{}^{18}O$ and $^1H^2H^{18}O$. The first molecule, $^1H_2{}^{16}O$, is most frequently found in nature with the others following respectively. In a water sample the enrichment of the rare molecule compared to the common one (D/H, $^{18}O/^{16}O$) is then measured as a ratio relative to an international standard.

3.1 The δ-scale

Isotopic measurements are recorded in the δ scale. That is calculated from the ratio R between the concentration of heavy and light isotopes in the sample (R_s) and the standard in the Vienna Standard Mean Ocean Water (VSMOW, the zero point in the δ-scale) R_{st} according to the equation:

$$\delta_i = \frac{R_s - R_{st}}{R_{st}} * 1000 = \left(\frac{R_s}{R_{st}} - 1 \right) * 1000 \qquad (3.1)$$

Since the values are relatively small the unit is in pro mil (‰, parts per thousand). From now on, $\delta^{18}O$ and/or δD will be used when referring to isotopic values.

3.2 Physical properties

Quantum mechanics controls the mass dependent equilibrium processes with the vibrational motion of the molecule being the most important factor in equilibrium isotopic fractionation. In that case the difference in isotope ratio can be explained by bond strength, the lighter isotopes have weaker bonds and thus take more readily part (less energy is needed) in a given reaction while the heavier ones sit tighter due to stronger bonds. Beside the mass effect, each isotopic atom and molecule has its own unique physical characteristics which control weather certain isotopes are enriched in the product or not. In nature, equilibrium processes occurs f. ex. in clouds forming precipitation where the

surrounding air is saturated with water vapor. It is also occurring just above the surface of a water body of any kind. Kinetic effects, also mass-dependent, are more visible in the global hydrological cycle since they occur on the integral scale, not the micro scale like equilibrium processes. That is specially the case during evaporation and deposition to form ice from vapor (Cappa et al., 2003).

3.2.1 Physical processes

When water vapor travels in an air mass along a certain trajectory, several parameters can affect the isotopic ratio. Landscape can alter the ratio of a precipitation in several ways. The δ value of a water sample decreases with both increasing latitude and altitude and with distance from coast. According to Árnason (Árnason, 1976), $\delta^{18}O$ decreases by -1‰ per latitude west of Greenland and δD by -8‰. Another important factor (also holding for both latitude and altitude) is the linear relationship between δD and $\delta^{18}O$, which was expressed by Craig in 1961 to be:

$$\delta D = 8 \cdot \delta^{18} O + 10 \qquad (3.2)$$

That is exposed in all meteoric water, except in places where evaporation is the main driving force (Craig, 1961), and has been of great use in hydrogeology. The lack of kinetic effects in the formation and deposition of snow is crystallized in this relationship (Dansgaard et al., 1973). Long term climatic variation, such as glaciations and changes in Earth´s orbit, leave a clear mark on the isotopic composition of precipitate. Like for the seasons the δ value is lower in cold periods than in warm periods, exposed in the oscillations observed in the $\delta^{18}O$ over several years, see fig. 3.1.

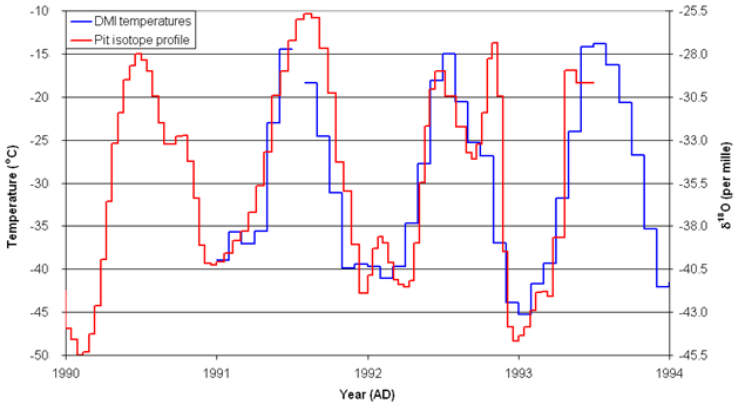

Figure 3-1: An example of the seasonal 18O signal observed in a GRIP pit core spanning 4 years. It´s correlation with temperature is also shown (Vinther, 2006).

Since precipitation is formed in clouds, the link between air temperature and water isotopes reflects the cloud temperature at the time of precipitation (Merlivat & Jouzel, 1979). Water isotopes can therefore serve as paleo thermometer. To convert water isotopes into air temperature (T_{air}), Johnsen et al. (1989) found the following empirical relationship, which best describes the present situation, to be:

$$\delta^{18}O = 0.67 T_{air} - 13.70‰ \qquad (3.3)$$

3.2.2 Deuterium excess

From $\delta^{18}O$ and δD the Deuterium excess (*d*), an informative climatic parameter, can be calculated from eq. (3.2):

$$d = \delta D - 8 * \delta^{18}O \quad (3.4)$$

According to Dansgaard (1964), the deuterium molecule is much less sensitive to kinetic effects than ^{18}O. That means that the $H_2{}^{16}O$ and $H_2{}^{18}O$ react more readily than $HD^{16}O$. The difference in the diffusivity between the three water molecules at the moisture source results in a slope of factor 8 under equilibrium conditions, as in eq. (3.2). When the enrichment of deuterium compared to that of ^{18}O in the delta scale (δ_D- δ_{18O}) is plottet relative to the slope 8 the d exess is revealed as a deviation from that slope. It is thus used as an indicator for non-equilibrium processes. Precipitation in high latitude costal areas has a present d value close to 10‰ (Johnsen et al., 1989), and mainly depends on the relative humidity (RH) *h* above the ocean as Merlivat & Jouzel (1979) pointed out. RH is the ratio between the water vapor content and the air´s capacity to hold vapor at a particular temperature and pressure and is often described in percentages. It also plays a crucial role in condensational/depositional processes in clouds.

Information on the origin of precipitation and physical conditions at the site of formation can be interpreted using d exess. Johnsen et al. (1989) did an important study on that subject and found evidence that showed that under present situation as well as during last glaciation, the precipitation in Greenland originates in the sub-tropical sea. At high altitudes changes in d exess have a few months lag time behind changes in $\delta^{18}O$ unlike the anti phase observed at lower altitudes (Johnsen et al. 1989).

3.3 Isotopic fractionation

The isotopic changes within a water droplet along its trajectory mentioned above, is explained by isotopic fractionation also known as isotopic distillation. Different fractionation processes affect the ever-changing phases and positions of the water molecule. Those dynamic processes influencing the droplet are not completely understood, thus simplified models are developed and used to approximate nature. Equilibrium isotopic fractionation arises mainly because of difference in vapor pressure between the three main water species, with the heavy molecules having lower vapor pressure (1% for H_2O^{18} and 10% for HDO), than the lighter one (H_2O^{16}) (Dansgaard et al., 1973).

3.3.1 Equilibrium fractionations

Equilibrium fractionation occurs in well-defined systems where number of water molecules is relatively constant over a period of time. Those systems can f. ex. be found in the liquid-vapor surface layers (saturation layers) of the ocean, a falling droplet, in clouds forming precipitation and when ice deposits from vapor (Cappa et al., 2003), as mentioned earlier. The formation of ice crystals starts when the relative humidity is 100 ± 1% with respect to liquid water (Jouzel & Merlivat, 1984). According to Dansgaard et al. (1973) evaporation from solids (sublimation) causes no isotopic fractionation. Thus, according to Dansgaard (1973) and Jouzel & Merlivat (1984), a simple fractionation model that neglects kinetic effects is therefore sufficient to explain the processes controlling the isotopic variations in snow.

An air parcel containing vapor moves upward to a height *h*. There it is directed towards higher latitudes where it condenses and the condensate falls immediately as precipitation when it forms. Dansgaard (1964) described such isotopic fractionation that occurs under those circumstances as Rayleigh condensation. Here, the snow is supposed to be formed in isotopic equilibrium with the vapor phase in the cloud before removal (W. Dansgaard, 1964), but many experiments have shown otherwise (Jouzel & Merlivat, 1984).

In an equilibrium process of evaporation-condensation (in the saturation layer), the isotopic ratio is defined as:

$$R_{liquid} = \alpha R_{vapor} \tag{3.5}$$

with the liquid being the ocean in this case. α is the fractionation factor and is dependent on the relevant isotopic species and the temperature *T*. By using eq. (3.1), eq. (3.5) can also be written as:

$$\frac{R_c}{R_{st}} = \alpha \frac{R_v}{R_{st}} \tag{3.6}$$

where R_c is the isotopic ratio of the condensate. And with some simple calculations using eq. (3.1) and (3.6), the relationship between temperature and the δ value is shown to be:

$$\delta_c + 1 = \alpha(1 + \delta_v) \tag{3.7}$$

3.3.2. Kinetic effect – evaporation

Above the saturation layer of the ocean is the boundary layer at height z with its turbulent and molecular mixing. There, equilibrium fractionation is no longer the governing process and kinetics take over. In Figure 3.2, the relevant layers schematically along with the controlling forces are shown.

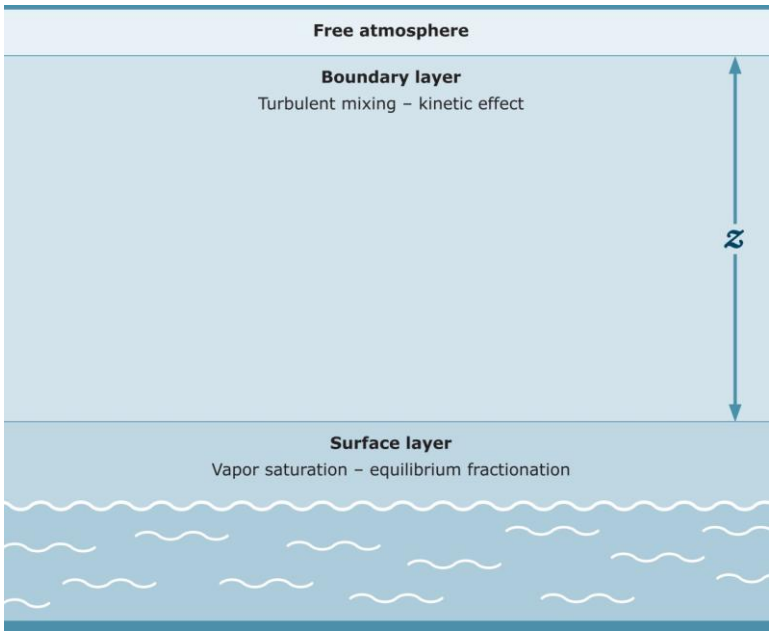

Figure 3-2: A schematic figure of the surface and boundary layers.

In the turbulent layer the flow of the molecules can be described by Fick´s law:

$$J = -D\frac{\partial n}{\partial x} \tag{3.8}$$

where J is the molecular flow , D the diffusivity and $\partial n / \partial x$ the density gradient. In words, Fick´s law describes the flow from high concentrated areas to ones less concentrated, with the magnitude of that flow being proportional to the concentration´s gradient.

In the boundary layer, according to Merlivat & Jouzel (1979,) the isotopic content of a water vapor leaving the surface ocean (v_0) depends mainly on the following parameters:

- α_e, a function of sea surface temperature T_e
- h, the relative humidity of the air masses formed
- k, a function of the wind regime in the boundary layer close to the surface of the ocean

In their model it is assumed that the atmosphere is in a steady state for the main three isotopic water molecules, meaning that the net fluxes of evaporation and precipitation is equal (dN_E=dN_P). Also, it is assumed that all the water in moist air masses is precipitated so that:

$$\delta_{v0}=\delta_P \tag{3.9}$$

Through the net flow E it is known that:

$$\frac{E}{\rho} = \Gamma\left(q_s - q\right) \tag{3.10}$$

where ρ is the density of air, q is the specific humidity at height z within the boundary layer and q_s is the saturated specific humidity at the air-water interface (z=0). Γ is the profile coefficient at z, defined as:

$$\Gamma = \frac{u_0}{\left(\rho_M + \rho_T\right)} \tag{3.11}$$

where u_0 is the friction velocity and ρ_M+ ρ_T are the molecular and turbulent resistance, respectively. Here, ρ_M is proportional to the –nth power of the molecular diffusivity D of water vapor in air and ρ_T includes the aerodynamic parameters. From eq. (3.10) & (3.11) an equation can be written for a specific isotopic molecule:

$$\frac{E_i}{\rho} = \Gamma_i\left(q_{si} - q_i\right) \tag{3.12}$$

Using equation (3.10) & (3.12) the isotopic concentration in the evaporating moisture can be calculated as:

$$R_E = \frac{E_i}{E} \tag{3.13}$$

In order to obtain the delta value, eq. (3.10), (3.12) and (3.13) is used along with eq. (3.1) to get:

$$1+\delta_E = (1-k)\left(\frac{\frac{1}{\alpha} - h\left(1+\delta_{v_0}\right)}{1-h}\right) \tag{3.14}$$

From eq. (3.14) and assuming an atmospheric steady state and that all water in moist air mass precipitates, the isotopic composition of the initial vapor can finally be deduced:

$$\delta_{v_0} = \left(\frac{1}{\alpha_e}\right)\left(\frac{1-k}{1-kh}\right) - 1 \tag{3.15}$$

Here it is obvious that the ratio is dependent on the three parameters stated above, where the relative humidity $h = q_s/q$ and $k = 1- \Gamma_i/ \Gamma$.

In order to define *k*, the relative difference between the molecular diffusivities in air needs to be introduced:

$$\varepsilon_D = \frac{D}{D_i} - 1 \tag{3.16}$$

From the z-profile coefficient in eq. (3.12), *k* can be defined as:

$$k = \frac{(1+\varepsilon_D)^n - 1}{(1+\varepsilon_D)^n + (\rho_M + \rho_T)} \tag{3.17}$$

which, as can be observed, is a function of the wind (turbulent) regime - including the molecular and aerodynamic parameters in the boundary layer.

3.3.3. Kinetic effects – precipitation

Kinetic effect controls the fractionation processes in vapor-ice transition leading to snow formation, opposed to the removal of it. Jouzel and Merlivat (1984) formulated a model in hope of getting a better agreement between theoretical and experimental results concerning the δD- $\delta_{18}O$ relationship and the temperature isotope gradient. This model is an extended Rayleigh model where a kinetic isotopic effect is taken into account. To define the kinetic effect, they assumed first that the condensation process takes place in a pure molecular regime. Knowing that and Fick´s law (eq. (3.8)) results in the surface flow *F* of $H_2{}^{18}O$ and HDO being proportional to (e_v-e_i), or:

$$F \propto D(e_v - e_i) \tag{3.18}$$

where D, e_v and e_i are the diffusivity in air, the partial pressure and the saturation vapor pressure over ice respectively. The vapor pressure ratio of the heavy (marked with ´) and light isotopes must be equal to the concentration ratio between the same species. With that in mind, an expression for vapor pressure of the surrounding vapor and for different isotopic species can be written as:

$$e'_v = e_v C_{smow}(1+\delta_v) \tag{3.19}$$

$$e'_i = \frac{e_i C_{smow}(1+\delta_v)}{\alpha_s} \tag{3.20}$$

α_s is the equilibrium fractionation coefficient (temperature dependent), C_{smow} is the isotopic ratio of the SMOW and δ_s is the isotopic content of the condensate at the surface. Unlike water, there is no isotopic homogenization in ice due to difference in the origin of the vapor depositing onto the ice crystal. The δ_s value is thus directly related to the ratio of the fluxes F (for H_2O) and F´(HDO, $H_2{}^{18}O$) through the relationship:

$$1+\delta_s = \frac{1}{C_{smow}}\frac{F'}{F} \tag{3.21}$$

which can also be written, using eq. (3.19) & (3.20) as:

$$1+\delta_s = \frac{D'(e_v(1+\delta_s) - \left(\frac{e_i(1+\delta_s)}{\alpha_s}\right)}{D(e_v - e_i)} \tag{3.22}$$

That simplifies to:

$$1+\delta_s = \alpha_k \alpha_s (1+\delta_v) \tag{3.23}$$

where α_k, the kinetic fractionation coefficient, is defined as:

$$\alpha_k = \frac{S_i}{\alpha_s \frac{D}{D'}(S_i - 1) + 1} \tag{3.24}$$

Here, S_i refers to supersaturation over ice, an important parameter during snow formation (Jouzel & Merlivat, 1984). With this new coefficient included in the Rayleigh model, $\alpha_k\alpha_s$ instead of α, discrepancies between model predictions and experiments were reduced and thus this model is one step closer to nature than before.

3.3.4. Diffusivity

Considering the importance of diffusivity (D) in isotopic processes, it needs a little more attention. Classical diffusion theory explains well the relationship between particle diffusivity (D_n) and mass. In order to study the particle density of the molecular flow J in Ficks law, the divergence of eq. (3.8) is calculated. That result in the differential equation:

$$\frac{\partial}{\partial t} n - D_p \nabla^2 n = 0 \tag{3.25}$$

which describes the distribution of particles in a given area over time. n is the particle density in m^{-3} and ∇^2 is the laplacian, the differential operator of the gradient ∇. When thinking of a left-to-right molecular flow, the molecular current J (net flow of molecules per unit area per time) can be described as:

$$J = (n_- + n_+)v \tag{3.26}$$

where n_- is the number of molecules on the left and n_+ the molecules on the right and v the velocity. (n_-—n_+) can be expressed using $n_a(x,y,z)$, the number density molecules in a volume element centered on (x,y,z), as:

$$(n_- - n_+) = \frac{\partial n_a}{\partial x}\Delta x = \frac{\partial n_a}{\partial x} 2l \tag{3.27}$$

Neglecting the factor 2 and substituting 3.26 and 3.27, the molecular flow can be described as:

$$J_x = -\frac{lv}{3}\frac{\partial n_a}{\partial x} \tag{3.28}$$

where the factor 1/3 is the result of careful theoretical analysis and $\partial n_a / \partial x$ is the density gradient. The same equation can be deduced for y and z respectively. By using Fick´s law (eq. 3.8) and substituting it into eq. (3.28) D_n can be written as:

$$D_n = \frac{1}{3} v_n l_n \tag{3.29}$$

where v_n is the mean velocity and l_n is the mean free path. Equation (3.29) also reveals the inverse mass dependence on temperature. However, in order to see that a damping factor γ must be introduced along with its inverse, $\tau = 1/\gamma$ describing the mean time between collision. The mean free path, the distance l between collision, can then be defined as $l_n = v\tau$. The damping factor also reveals the molecular drag γm, where m = mass, and its inverse being the mobility $\mu = 1/\gamma m$. Having defined the above terms, the relationship can be written as:

$$D_n = \frac{1}{3} v_n l_n = \mu k_b T = \frac{k_b T}{m\gamma} \tag{3.30}$$

where k_b is the Boltzman constant and T temperature. From eq. (3.30), the inverse relationship between particle diffusivity and mass is observed. Equation (3.25) is quite fundamental since it can be used both for thermal and particle diffusion. It is thus also used to calculate diffusion in firn/ice that is discussed in part 3.4.

3.4. Diffusion

When snow settles on the ice sheets layer upon layer it condenses due to the overlying weight. Such condensation can strongly affect the isotopic profile. Herron and Langway (1980) (Herron & Langway Jr, 1980), first described the three stages in firn-ice transition. The densification from the initial snow density to the critical density of 550kg/m^3 is referred to as the first stage. It occurs more rapidly than the other stages and grain settling and packing is the dominant mechanism. In the second stage the rate of densification occurs more slowly as the depth increases. At the maximum depth in the second stage, the pore close-off zone, the intercommunicating air passages closes to form individual bubbles of density between 820-840 kg/m^3. The third stage occurs below the pore close-off zone. There, air can no longer enter and further compression of bubbles along with densification takes place. Glacier ice has formed with the maximum density of 917 kg/m^3.

High frequency isotopic variations in firn are removed due to strong smoothing processes. The diffusion length in firn, the length that a molecule can move in the firn due to diffusion, was calculated by Johnsen (1977) (although not quantitatively correct due to assumptions made) as being the vertical displacement:

$$L_f^2 = \frac{c_2}{c_1} D(v_{p_0} - v_p) \tag{3.31}$$

Where D is the diffusion constant of water molecules in air, c_1 and c_2 are constant and v_p and v_{p0} is the volume of pore space and initial pore space respectively. Johnsen (1977) also described the smoothing effect of the diffusive transport in firn as being the ratio R between the final and initial $\delta^{18}O$ amplitude with a wavelength λ in cm:

$$R = \exp(-2\pi^2 \frac{L_f^2}{\lambda^2}) \tag{3.32}$$

A slightly modified version of this equation resulted in the average displacement of water molecules, both from Greenland and Antarctica, being 7-8 cm from the initial position after firnification.

The smoothing then proceeds below the firning zone where general strain rates and solid ice diffusion smooths the remaining isotopic signal. The depth of the firn-ice transition in the shallow NEEM S2 2008 core is 60m but only 40m are presented in this thesis, the ice diffusion does not play a role.

3.4.2. Reversed diffusion

Deconvolution, or reversed diffusion, is a technique also developed by Johnsen (1977) to reconstruct the initial frequency of the isotopic profile. It uses the concept of convolution (diffusion) which is basically when two functions combined yield a third function. The third function is thus modified from the initial two.

Going back to part 3.3.4, the solution of the differential eq. (3.25) and knowing the start profile (x,0), results in the known convolution integral:

$$\phi(x,t) = \frac{1}{\sqrt{4\pi Dt}} \int_{-\infty}^{\infty} e^{-\frac{(x-y)^2}{4Dt}} \phi(y,0)dt \qquad (3.33)$$

The solution of eq. (3.33) results in the symmetrical filter F_1:

$$F_1 = \exp\left(\frac{-\frac{1}{2}(z-z')^2}{L^2} \right) \frac{1}{L\sqrt{2\pi}} \qquad (3.34)$$

That is, the effect that a diffusion has on a $\delta^{18}O$ profile is shown to be equivalent to convolving (modifying) the profile with a symmetrical filter F_1. The transfer function (the function that describes how each frequency is modified through the core) of F_1has the equation:

$$\overline{F_1}(k,L) = \exp\left(-\frac{1}{2} k^2 L^2 \right) \qquad (3.35)$$

where $k = \frac{2\pi}{A}$ is the wave number, L the diffusion length and $\overline{F_1}$ the Fourier transform of F_1.

Different deconvolution filters can be derived from eq. (3.35), depending f. ex. on the noise and the sample length of the ice core data in question. Profiles that have high frequency data needs to undergo strong damping so the noise will not suffocate the relevant profile if blown up the scale. That can be accomplished by using the optimum Wiener filter design.

The measured high frequency profile can then be described as a sequence of numbers, or:

$$\delta_{mi} = \delta_{ai} + \epsilon_i \qquad (3.36)$$

where ϵ_i is noise (usually between 0.1 and 0.2‰) and δ_{ai} the value required.

The transfer function of the optimum Wiener filter is then necessary to retrieve the δ_{ai}:

$$\overline{F_2} = \frac{\left|\overline{\delta_a}\right|^2}{\left|\overline{\delta_a}\right|^2 + \left|\overline{\varepsilon}\right|^2} \qquad (3.37)$$

4 Sample handling and measurement tecniques

The 80 m long NEEM S2 08 shallow core was cut into 55 cm bag samples. Each bag sample was then cut into 2.5 cm sample to get a seasonal resolution. The samples were melted in Copenhagen and sent to Reykjavik, Iceland, in small plastic bottles refrozen. The samples were analyzed for stable water isotopes at the Institute of Earth Sciences in Reykjavik, using a Delta V Advantage mass spectrometer and a Picarro analyzer for isotopic H_2O. In this chapter the main functions of the devices used will be discussed along with concepts related to the mass spectrometer. Results on different measuring techniques will also be presented.

4.1 The IRMS

The Delta V Advantage is an Isotope Ratio Mass Spectrometer (IRMS), primarily designed to measure isotopic mass-to-charge (m/z) ratios of lighter elements that can be transformed into gaseous substances. An ion source, located in the ion chamber, ionizes the sample gas. That occurs when a beam of electrons from a tungsten filament inside the source collides with the gas. There, the ions are accelerated to 3keV and directed into a beam by a magnetic field which then enters the magnet by a 2mm slit. The lower (lighter) the isotopic m/z ratio is, the quicker the ion sways off track (fig. 4.1). A Faraday collector (cup), a current generating metal structure, then collects the appropriate ions.

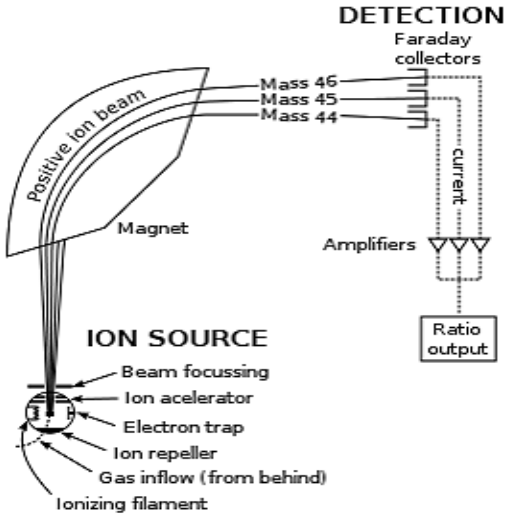

Figure 4-1: The inside of the IRMS here shown along with the mass-dependent path from the ion chamber to the output signal (U.S Geological Survey, 2013).

A HD collector system (a dual faraday collector) is used when analyzing HD isotopes, and a universal triple faraday collector when measuring heavier isotope ratio like $^{16}O/^{18}O$. The current is then amplified and converted into frequency, leaving the MS as a radio signal. In

the computer, the radio signal is again converted from frequency to voltage (mV). When the signal has been converted to voltage it is then interpreted into relevant isotopic ratio, expressed as:

$$R = \frac{Heavy\ Isotope}{Common\ Isotope} \quad (4.1)$$

The computer software calibrates the isotopic ratio of the reference gas by comparing it to a known standard. That is also practical in order to eliminate any instrumental errors. In the case of stable water isotopes, Vienna Standard Mean Ocean water (V-SMOW) is used. There are several ways to inject the sample into the MS via different inlets. The inlets that are used at the Institute of Earth Sciences are High Temperature Elemental Analyzer (TC/EA) coupled to a Continuous Flow (Conflo) inlet, and a Gas Bench device.

4.1.1 TC/EA

In the TC/EA, a liquid sample is injected into a 1393°C furnace. There, the sample vaporizes and separates into its molecular components (in this case H_2 and O). The oxygen reacts with a glassy carbon reactor, positioned in the TC/EA, to produce CO. Helium gas, continuously flowing, then carries H_2 and CO into the Gas Chromatographic (GC) column (fig. 4.2). There the molecules are further separated due to mass, with lighter molecules traveling faster than the heavier ones before arriving in the Conflo. The

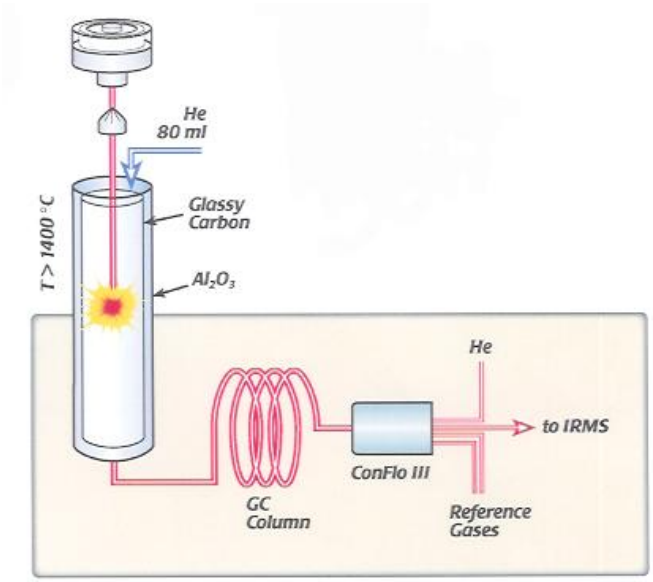

Figure 4-2: TC/EA inlet and the path the sample takes before entering the IRMS.

The basic concept of the Conflo is to reduce the amount of gas that enters the IRMS. The flow from the TC/EA is usually between 80-100ml/min but when it goes through the Conflo it is ~10ml/min which allows for a higher instrumental precision. It also dilutes gases if necessary and injects the reference gases, CO and/or H_2, for oxygen and hydrogen isotopes measurements respectively. TC/EA do offer the possibility of simultaneous measurements of hydrogen and oxygen isotopes. In the Conflo, there are two tubes, one for the sample (the sample section) and one for the reference gases (the reference section). From there the sample gas is transported into the mass spectrometer through the needle

valve where it enters the ionization chamber. The IRMS offers very good precision when using TC/EA Conflo inlet, with internal precision of 0.08 ‰ when measuring ^{18}O and 0.40‰ with ^{2}H.

The calibrated raw data from the TC/EA (stored as an excel file) needs to undergo several corrections before the true values are revealed. First, the syringe in use has a very small volume (2-5µl) so the measurements are very sensitive to any volume fluctuations that need to be corrected for. Small fluctuations are normal but any unusual fluctuations are most often related to the syringe. The reason can be a wrong method describing the wrong syringe and volume to be injected or a clogged needle. When different samples are being measured, a memory effect occurs, which also needs to be corrected for. That is when there is a leftover in the syringe/analyzer from the previously measured sample that can affect the value of the next sample. In order to prevent that, samples and standards need to be measured number of times. The number of injections in each vial depends on the value of the previous sample/standard. The corrections for the IRMS are done using a MATLAB script written by Bo Vinthers at the Nils Bohr´s Center for Ice and Climate in Copenhagen.

4.1.2 Gas Bench

In the Gas Bench, the technique and sample handling are quite different. The liquid water samples are put in vials (200µl sample in 12ml vials) where they are flushed with appropriate flush gas, depending on what is being measured. The flush gas used for ^{18}O measurements consists of 99.7% He and 0.3% CO_2. After flushing it requires a reaction time of at least 24 hours prior to measuring (see appendix I for more information). The flush gas used for ^{2}H measurements consists of 98% Helium and 2% Hydrogen. The reaction time after flushing is 1 hour minimum. For hydrogen measurements a titanium stick is inserted in each vial that serves as a catalyst and thus speeding up the reaction between the flush gas and the sample.

The Gas Bench is much more vulnerable to diurnal and seasonal temperature changes than the TC/EA. This is recorded in a trend that can be observed in the data. With that in mind the right temperature balance is crucial. The vials are in a tray that is set to 21.5 – 22.5°C (just above room temperature which is between 18-19°C).

After the flush gas has reacted with the sample and a routine calibration test has been done (see part 4.3) the measurement can begin. Then the gas mixture gets transported from the vials into a water trap before entering the valco valve (see fig. 4.3). In short, a valco valve controls the sample volume, or pulses, that go into the GC column. Another water trap awaits the sample gas when it exits the GC and enters the open split where it is finally injected into the MS.

The memory effect is not a problem in the Gas Bench. The valco valve controls the amount and frequency of the sample that goes into the MS. One sample is thus measured ten times (ten peaks as seen in fig. 4.3). The average of eight is then used to calculate the δ-value. To be precise, the first peak and the last are removed and those in between are used to calculate the average value. Those calculations are done in excel. Since the valco valve controls the amount of sample that goes into the MS, volume fluctuations are not a problem in the Gas Bench and thus need not to be corrected for.

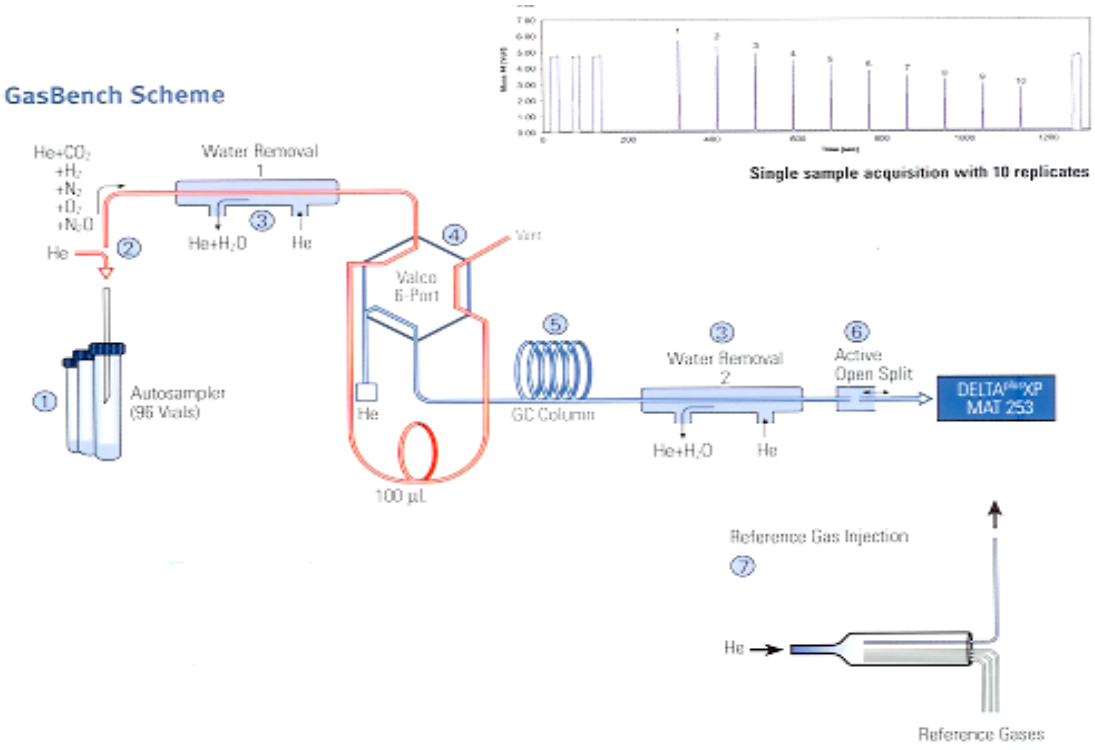

Figure 4-3: A schematic picture of the sample path in the Gas Bench along with the output signal as shown on screen (in mV).

4.2 Calibration and precision

The measurement precision obtained at the Institute of Earth Sciences, are below 1.0‰ for δD and below 0.1‰ for $\delta^{18}O$. That is a little higher than the instrumental precision. In order to keep both the instrumental and measurement precision relatively constant over time, routinely tests are necessary. Some tests are only required once in a while, such as the magnetic scan. By choosing a relevant cup, it is possible to observe what the magnet is really detecting. That´s how a leakage could f. ex. be detected. Part of the IRMS frequent measuring procedure is the linearity test using a reference gas, also referred to as an On Off test. It measures how linear the values of ten pulses are. A different reference gas is used depending on which isotopes will be measured. The standard deviation (std) of those ten peaks is then calculated. A std below 1.0 for δD and below 0.1 for $\delta^{18}O$ is acceptable, the same as with the measured precision.

Two different methods are used when producing hydrogen, both with different isotope $^2H/H$ ratio. They are electrolysis (3:1) and hydrocarbons (5:1) the latter is used at the Institute of Earth Sciences. The $^2H/H$ ratios that are measured in water and glacier samples differ quite from the one in the reference gas. That can lead to a decrease in precision. When using ^2H reference gas in hydrogen measurements in the IRMS, an inconvenient chemical reaction occurs in the ion source:

$$H_2^+ + H_2 \rightarrow H_3^+ + H$$

The H_3^+ ion has the same mass, and m/z, as HD which can cause obvious problems. To avoid that unbalance, resulting in a bias in the isotope ratio, a routine H_3 On-Off test is

done. That is similar to the linearity test mentioned above but with an additional H_3 factor calculated. The H_3 On-Off test measures ten pulses of reference gas, each having different concentrations that grow linearly. The concentrations are controlled by increasing (by hand) the pressure on the reference gas, usually from ~0.5-2.5bars.

4.3 The Picarro

The Picarro instrument was installed late August and thus not many samples from the NEEM S2 08 shallow core were measured on it compared to the IRMS. Though good results were obtained it still needs some tuning.. The advantage of the Picarro is that it is user friendly and measures $\delta^{18}O$ and δD simultaneously with similar precision as the IRMS does.

4.3.1 Technique

The instrument consists of High Precision Vaporizer and an auto sampler connected to an analyzer. Two vacuum pumps secure stable pressure. The sample is injected into the vaporizer through a 5µl syringe attached to the auto sampler. After it evaporates, the sample is then directed into the analyzer. A special analyzing technique that is utilized and developed by Picarro is referred to as Cavity-Ring-Down Spectroscopy (CRDS) (fig. 4.4). CRDS takes advantages of the fact that nearly every gas molecule has its own unique near-infrared absorption spectrum of certain wavelength which can then be analyzed. In conventional infra-red spectrometers, the absorption strength of trace gases can be difficult to measure due to their short wavelength. The CRDS avoids that problem by increasing the wavelength in question, thus increasing the precision and accuracy of the measurements. In the CRDS, a laser beam enters the cavity that consists of three mirrors. Quickly the cavity fills with laser beams which a small photo detector senses through a leakage in the mirror. It then produces a signal that is directly proportional to the intensity in the cavity. After a few tens of microseconds the laser turns off and the bouncing beams leaks out exponentially until zero is reached. This decay, called „Ring down“, is measured by the photo detector but the time it takes is determined by the reflectivity of the mirrors.

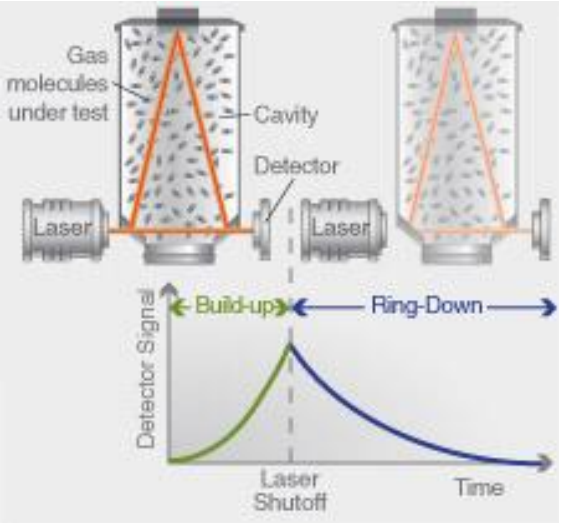

Figure 4-4: CRDS system and the Ring down (Picarro, 2012).

When absorptive gas species are introduced into the cavity the Ring down time will decrease. Thus a comparison between sample-free cavity and the reference cavity is possible, (fig. 4.5) producing precise and quantitative measurements. Since the Ring down time is only used, the data is independent of laser intensity fluctuations or absolute laser power.

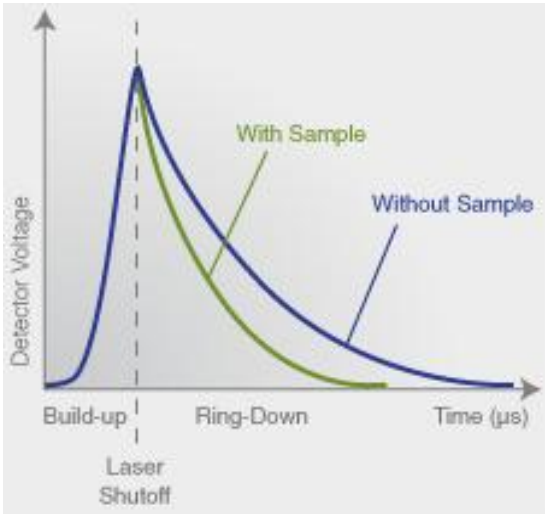

Figure 4-5: Difference between the Ring-down timing with and without sample (Picarro, 2012).

4.3.2 Measurements and methods

Both samples and standards were injected into 0.5ml vials with the 0.5µl syringe. Three standards were used, -40‰, -22‰ and a NEEM standard. A memory effect, the same as is described for the TC/EA, is also a problem when using the Picarro. The difference between -40‰, -22‰ and the NEEM standard is quite large so they need to be measured more often than the samples. Here it was estimated that 15-20 times was enough to eliminate the memory effect. Since all the samples were glacier water, 8 times was considered to be enough. The memory effect can be observed and estimated when the run is calculated in a specific Picarro MATLAB script, written by Steen-Larsen (2012). To eliminate the memory effect, parts of the measurements are removed when estimating the average value for each sample. In the case of the standards, the first 10 out of 15 values were removed and the rest used in the data analysis but the first 4 values of 8 in case of the glacier samples.

4.3.3 Precision

The calculated sample values depend on the accuracy of the standards measured in the beginning of each run. A difference between the known value and the measured value of the third standard (the residual) is thus calculated to estimate the accuracy of the whole run. If the residual is below 0.1‰ for $\delta^{18}O$ and 1.0‰ for δD, the run is considered to show satisfying results. The typical instrumental precision in the Picarro allows for 0.07 ‰ for $\delta^{18}O$ which is similar to the IRMS. For δD the precision is 0.2‰, thus outperforming the IRMS.

Throughout the run, the NEEM standard (can be other relevant standard) is placed as test sample, usually after every ten samples. MATLAB then calculates the residual on those test samples too. Like the residual on the third standard tells of instrumental precision, the test residuals can tell if the precision is time-dependent. During the interval of the Picarro measurements, the test samples were not always placed in each run. In table 4.1, the residuals of standard 3 and the test samples (if present) is shown. The number of test samples depends on the number of unknown samples.

Table 4-1: The changes of residuals with time and length. Not all runs had test samples and the run length varied, explaining the emty rows and seats.

Picarro runs:	**Sample Residual:**		**Test residuals:**										
Date	δ18O	δD	#1 $\delta^{18}O$	#1 δD	#2 δ18O	#2 δD	#3 δ18O	#3 δD	#4 δ18O	#4 δD	#5 δ18O	#5 δD
12.8.2012	-0,04	-0,05	0,00	-0,01	-0,04	0,06						
14.8.2012	0,05	0,32										
23.8.2012	0,01	0,26	0,04	0,26	0,09	0,51						
30.8.2012	0,13	0,57	0,07	0,36								
3.9.2012	0,00	0,02										
5.9.2012	0,05	0,41										
10.9.2012	0,06	0,73										
12.9.2012	0,01	0,60										
14.9.2012	-0,10	-0,22										
17.9.2012	-0,01	0,06										
19.9.2012	-0,03	0,13	-0,11	-0,45								
21.9.2012	0,06	0,70										
3.10.2012	-0,11	0,22	-0,12	0,16	-0,15	0,18	-0,13	0,32				
5.10.2012	-0,12	-0,15	-0,11	-0,43	-0,09	-0,23	-0,15	-0,56	-0,16	-0,37	-0,15	-0,38
14.10.2012	0,04	0,51	0,00	0,18	-0,06	0,18	-0,04	-0,14	0,01	0,71		
18.10.2012	0,00	0,27	-0,03	0,01	-0,05	0,14	-0,11	-0,13	-0,08	0,17	-0,15	-0,38
Average:	0,00	0,27	-0,03	0,01	-0,05	0,14	-0,11	-0,13	-0,08	0,17	-0,15	-0,38

The ideal system should be linear, meaning that there should be equal amounts of negative residuals as there are of positive residuals. In other words, the average of the residuals should be zero. As can be seen in table 4.1, that is the case with the standard residuals of $\delta^{18}O$ but not for δD. However, the sample residuals are well within limits of the estimated instrumental precision and the same can be said with the test residuals, although being slight higher. The results presented in table 4.1 thus show that the results from the Picarro are reliable.

4.4 Instrument comparison

The result difference between the instruments described in chapter 4 is demonstrated in this part. Table 4.2 show an example of the same set of samples being measured with different instruments and demonstrates the reliability of the results. As can be seen in the difference, the $\delta^{18}O$ values between the GB and the Picarro don´t show much difference except in sample 06-03. The average is also within measurement precision. More difference exists in the δD values, where 4 samples have quite high difference. The average difference in the δD values is a litle higher than expected. However if sample 06_01 is treated as an outlayer the average becomes 0.74 which is also below measurement precision.

Table 4-2: Results showing the same samples measured for $\delta^{18}O$ in the GB and the Picarro and for δD in the TC/EA and the Picarro and the resulting difference between instruments.

	$\delta^{18}O$			δD		
Sample nr.	GB	Picarro	Difference	TC/EA	Picarro	Difference
05_08	-38,04	-37,91	-0,13	-293,42	-292,83	-0,59
05_09	-37,73	-37,68	-0,05	-292,97	-291,74	-1,23
05_10	-37,46	-37,40	-0,06	-288,80	-287,98	-0,82
05_11	-36,62	-36,53	-0,09	-280,69	-280,20	-0,49
05_12	-35,38	-35,28	-0,10	-269,66	-268,86	-0,80
05_13	-33,95	-33,89	-0,06	-257,63	-256,83	-0,80
05_14	-32,95	-32,87	-0,08	-248,13	-247,41	-0,72
05_15	-32,20	-32,10	-0,10	-241,96	-241,24	-0,72
05_16	-31,74	-31,68	-0,06	-238,83	-238,25	-0,58
05_17	-31,34	-31,30	-0,04	-236,39	-235,82	-0,57
05_18	-30,81	-30,70	-0,11	-232,17	-231,60	-0,57
05_19	-30,04	-29,91	-0,13	-226,38	-224,83	-1,55
05_20	-29,51	-29,58	0,07	-223,03	-222,49	-0,54
05_21	-29,46	-29,38	-0,08	-222,88	-221,79	-1,09
05_22	-29,29	-29,22	-0,07	-222,57	-221,11	-1,46
06_01	-28,92	-28,84	-0,08	-221,98	-219,22	-2,76
06_02	-28,99	-28,90	-0,09	-220,01	-218,93	-1,08
06_03	-28,85	-28,67	-0,18	-219,08	-217,48	-1,60
06_04	-28,70	-28,69	-0,01	-218,35	-218,60	0,25
06_05	-29,17	-29,15	-0,02	-222,94	-222,96	0,02
Average:			0,07			0,88

5 The NEEM 2008 S2 shallow core. Results

1585 samples of the NEEM 2008 S2 (NEEM08S2) shallow core, covering 39.6 m, were measured from June 2011 to October 2012. In this chapter the $\delta^{18}O$ and δD profiles are presented on a depth and age scale. The deconvoluted profile and the d excess were used to construct the age scale and are thus also presented. The temperature was estimated from the $\delta^{18}O$ value and annual and seasonal temperature profiles studied.

5.1 The isotopic data set

In fig. 5.1, the linear relationship of the measured samples is displayed. According to eq. (3.2), the slope of the world Meteoric Water Line is 8 However, due to kinetic effects and other factors influencing the isotopic values of precipitation the slope can vary slightly.

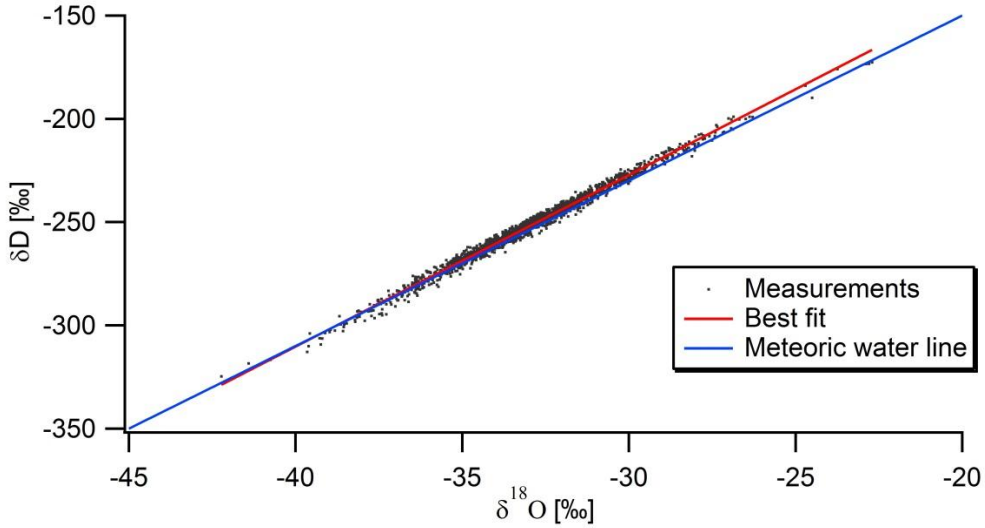

Figure 5-1: The linear relationship of δD and $\delta^{18}O$ of the NEEM 2008 S2 shallow core.

The equation for the line that best describes the dataset is $\delta D = 8.30\delta^{18}O + 21.32$ and the correlation between δD and $\delta^{18}O$ is very high, with $R = 0.99$. In fig. 5.1 the data range is quite visible, with the $\delta^{18}O$ values mostly between -40 and -25 ‰ and the δD between -320 and -200 ‰.

In figure 5.2, $\delta^{18}O$, δD and the d excess are presented on a depth scale. The linear relationship between the stable water isotopes is displayed in very similar profiles between $\delta^{18}O$ and δD, although the Y-scale differs. The d excess has a seasonal variation which should be relatively uniform at present, with values in the range of 5-15 ‰. The average d value of the NEEM08S2 data is 11.85 ‰. That is somewhat higher than in other Greenland ice cores but similar to the 11.5‰ value of the NEEM0703 value from Steen-Larsen et al. (2010).

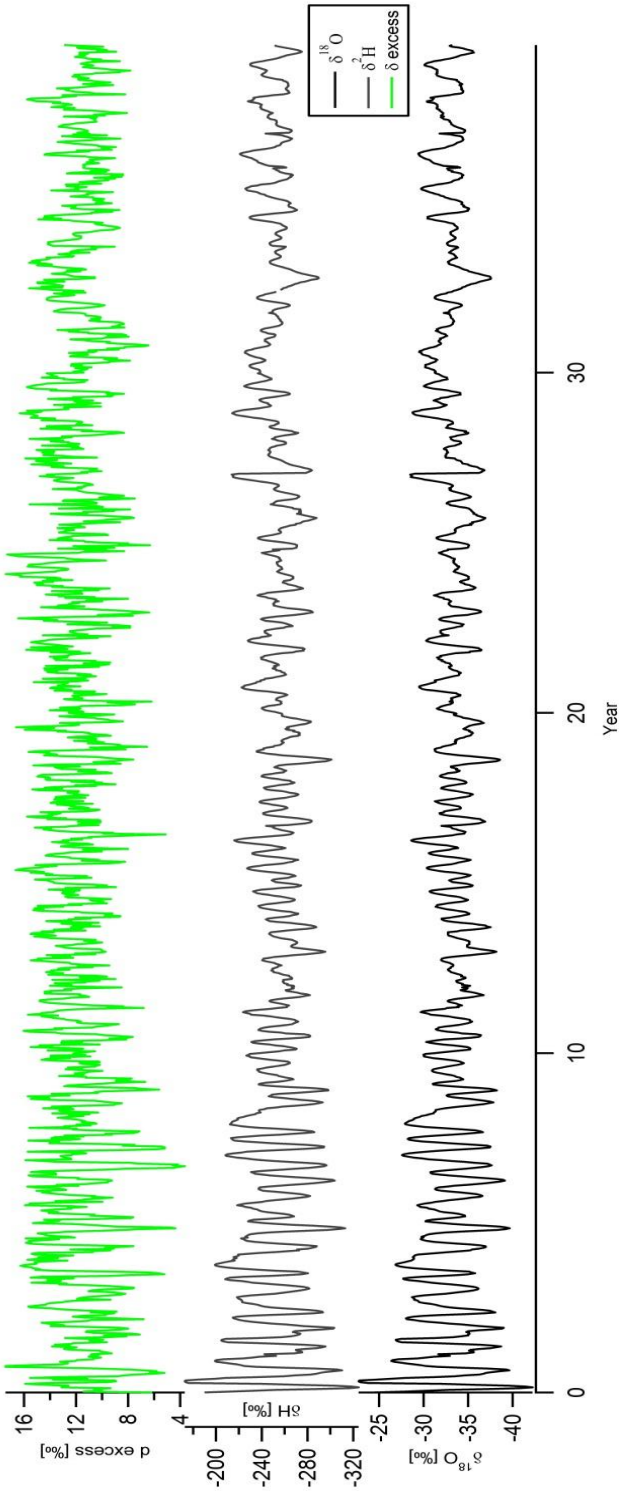

Figure 5-2: $\delta^{18}O$ (gray), δD (black) and the d excess (green) plotted on a depth scale. There are still some outliers that need to be re-measured. They are most obvious in the d excess profile.

5.2 The age scale

The age scale for the NEEM08S2 shallow core was constructed based primarily on counting deconvoluted $\delta^{18}O$ annual signals. d excess values and Electrical Conductivity Measurements (ECM), measuring the acidity of the ice, was used for reference. A comparison with the isotopic profile of NEEMS3A08 shallow core was also used.

CM profile acid peaks normally refer to certain volcanic eruption. Most large peaks have been identified in earlier Greenland deep cores but some are still unknown. Acid peaks observed in the upper part of the firn are not always reliable (Vinthers, personal communication) and thus comparison between the ECM profiles of the shallow cores is important. Some eruptions are not recorded in the ECM and some show delay from the eruption itself to the arrival of the signal. Couple of important factors control that, f. ex. the location and timing of the eruption along with the size and height of the plume. If the plume enters the stratosphere, ash aerosols and sulfur particles can spread over long distances and can thus be recorded far away.

ECM comparison between the shallow cores NEEM 2008 S3, S1 and S2 revealed false peaks in the shallow part of NEEM08S2 ECM record, see fig. 5.3. The ECM peak at 35,4m depth has been identified as the 1912 Novarupta-Katmai eruption (Vinthers, personal communication) and is identified in all of the shallow cores. It was one of the biggest eruptions in the 20th century and has left a distinctive ECM peak in the Greenland ice cores, giving a very valuable fixed time horizon. Another fix point was the year 1983, known for its cold summer. It had been identified in the NEEMS3A08 and NEEM07S3 shallow cores at 11.80m depth. The counting error down to the year 1964 is none, since the layers are relatively clear in that interval. From the year 1964 down to 1902 the error is estimated to be ±1 year.

In figure 5.4, the $\delta^{18}O$ profile is presented on the constructed age scale. The climatic variability visible in the profile will be discussed after the temperature reconstruction.

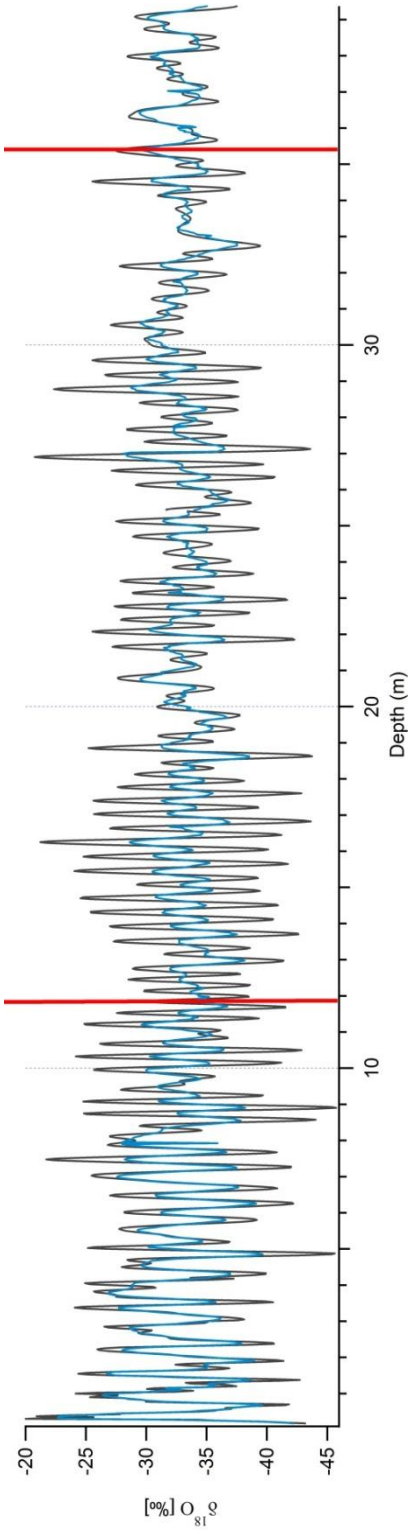

Figure 5-3: The raw and deconvoluted profile (blue and gray) $\delta^{18}O$ profile. The red lines indicate fixed points used.

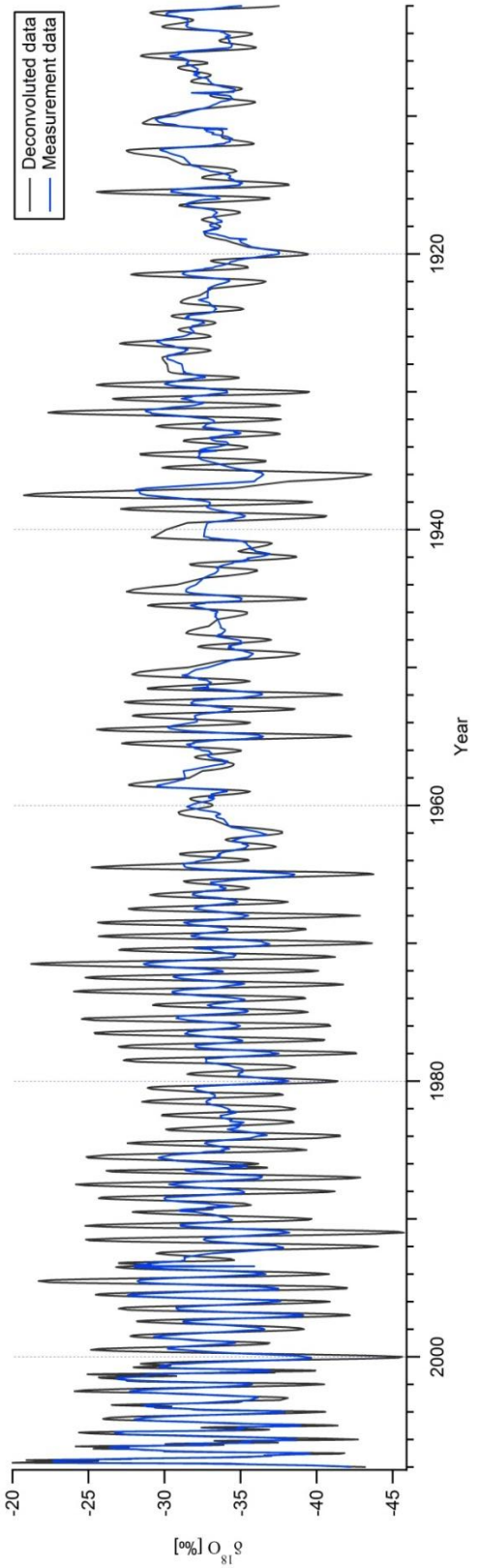

Figure 5-4: The $\delta^{18}O$, raw (blue) and deconvoluted (gray) profiles constructed on an age scale.

5.3 Temperature reconstruction

The isotope- temperature relation has been empirically described by Johnsen et al. (1989) to best fit the present climate situation, as discussed in chapter 3.

The isotope-to-temperature conversion is easy to calculate by using equation 3.3. The results are shown in figure 5.5 both for the deconvoluted and raw profile.

Gradual cooling starting in 1919 is visible, reaching a peak in 1920. The summers between 1920 and 1930 show relatively higher temperature, also known in the instrumental record as the warm decades between 1920 and 1940. Interesting climatic event seems to be occurring in the years around 1960 where little temperature difference seems to be between seasons.

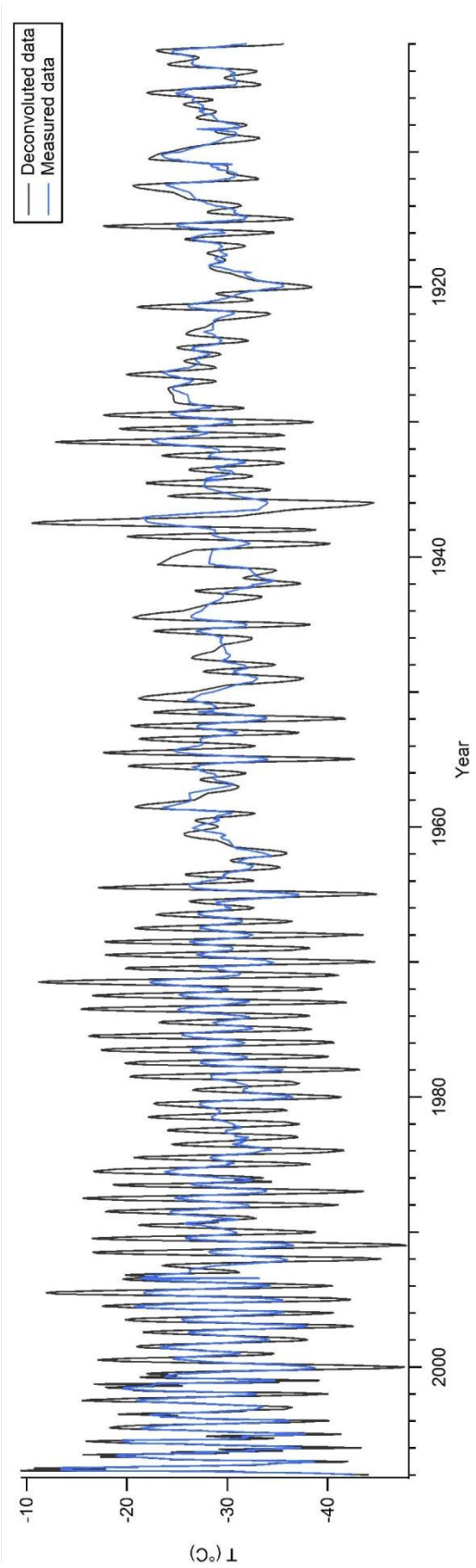

Figure 5-5: The isotopic temperature profiles of the deconvoluted (grey) and the raw (blue) data.

5.4 Annual and seasonal signal

The study of the annual and seasonal signal can be informative. $\delta^{18}O$ is a fundamental temperature proxy and as such it gives relatively good, independent information. In this part the annual profile along with the seasonal profiles are presented on a temperature/age scale.

In order to retrieve the annual signal, the average isotopic value between two winter peaks is calculated. This is demonstrated in fig. 5.6. Winter peaks have the lowest (lightest) isotopic values while the summer peaks have the highest (heaviest). Unlike the annual profile, the seasonal signal is constructed by using the deconvoluted values. However, the example of the seasonal signal given in fig. 5.6 is based on raw values.

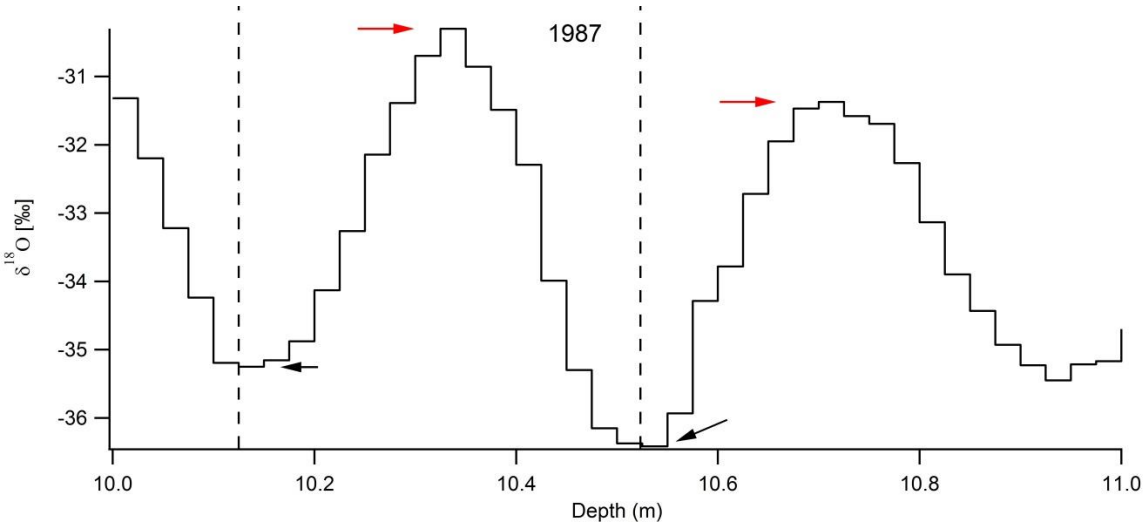

Figure 5-6: Between the dotted lines is the annual isotopic layer of 1987 occurring between 10 and 11 m depth in the NEEMS208 shallow core. For clarification red arrows point at summer peaks and black arrows to winter peaks.

The mean annual temperature profile presented in fig. 5.7 reveals interesting features. The known warm period between 1920´s and 40´s can be observed along with gradual warming from the beginning of 1980. Another interesting feature is the 20 year cycles that disappears after 1980, showing more negative $\delta^{18}O$ values around the years 1920, 1944, 1962 and 1984. When the temperature is studied between 1980 and 2007 the average temperature rise is found to be 2.5°C in the NEEM area, or 0.093°C/year.

The average rise in global temperature during the past decades is well known (Hansen et al., 1981), while the reason behind it is still debated.

The seasonal profile, presented in figure 5.8, can offer a possible explanation. Unlike the annual profile, the seasonal profile was constructed by taking the heaviest summer value and the lightest winter value per year. When looking at the change in summer temperature for the 20th century similar patterns occurs as in fig. 5.7. The warm period in the 1920´s and 30´s is visible as a curve both in the summer and winter profiles, but the 20 year cycle is not as obvious as in the annual signal. Since the cycle seems to start and end in a cool average year, it it seems that cool summers appear approximately every 20 years. The seasonal signal also seems to be in anti phase in that same interval. After 1980 a gradual temperature rise in the summer profile takes place, also observed in the annual figure (5.7).

However, the winter temperature shows unexpected trends after the mid 20th century. According to the winter profile temperature gradually falls after 1980´s, indicating cooler winters (-0.15°C/year) at the same time as the summers are getting warmer (0.2°C/year).

Figure 5.9 show a more detailed view of the d excess profile of NEEM08S2 at depths between 8 and 11m along with the $\delta^{18}O$. An example of the seasonal signal in the d excess profile is then observed along with the seasonal difference between the two profiles. The dashed lines there between indicate a lag time of 2-3 months which is consistent with known lag time in Greenland (Johnsen et al. 1989).

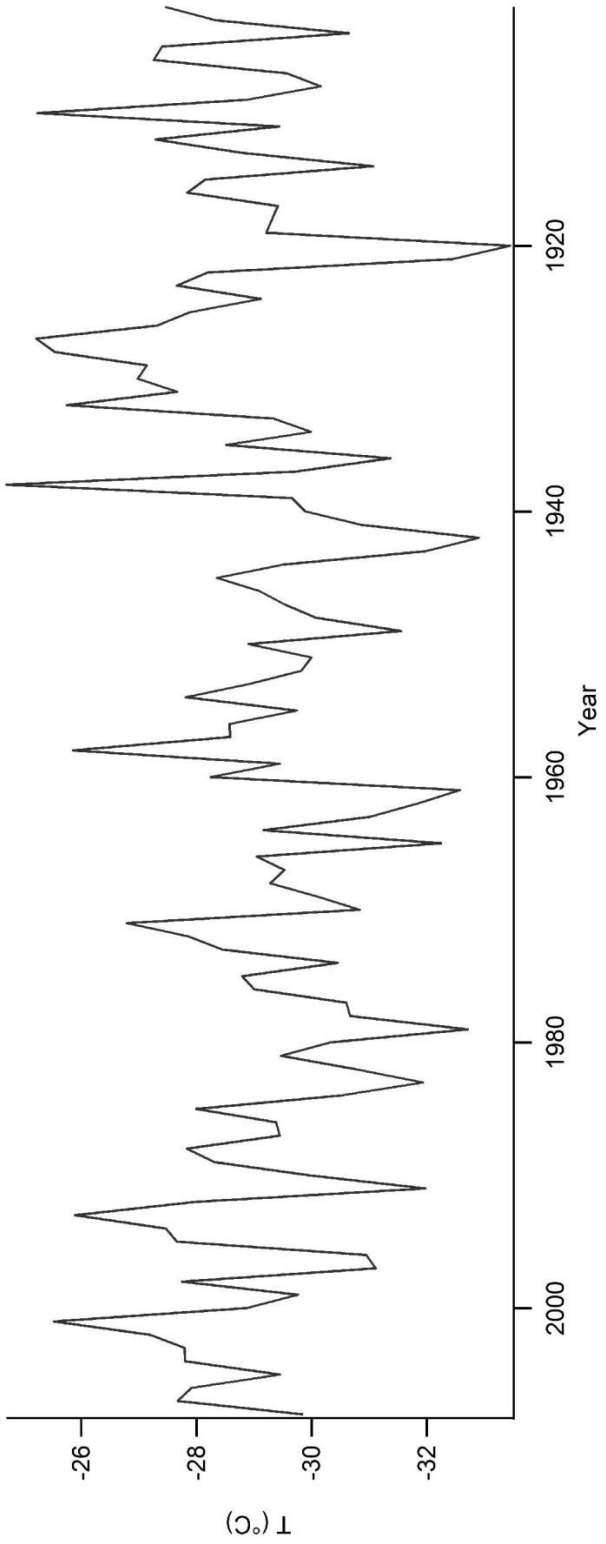

Figure 5-7: Mean annual isotopic profile from 1902-2007. The cold decades between 1920 and 1940 are also observed with the 20 year cycle repeating until 1984. After that is a clear trend. When the temperature is studied between 1980 and 2007, the average temperature rise is 0.093°C per year in the NEEM area, equivalent to 2.5°C rise for the æast 27 years.

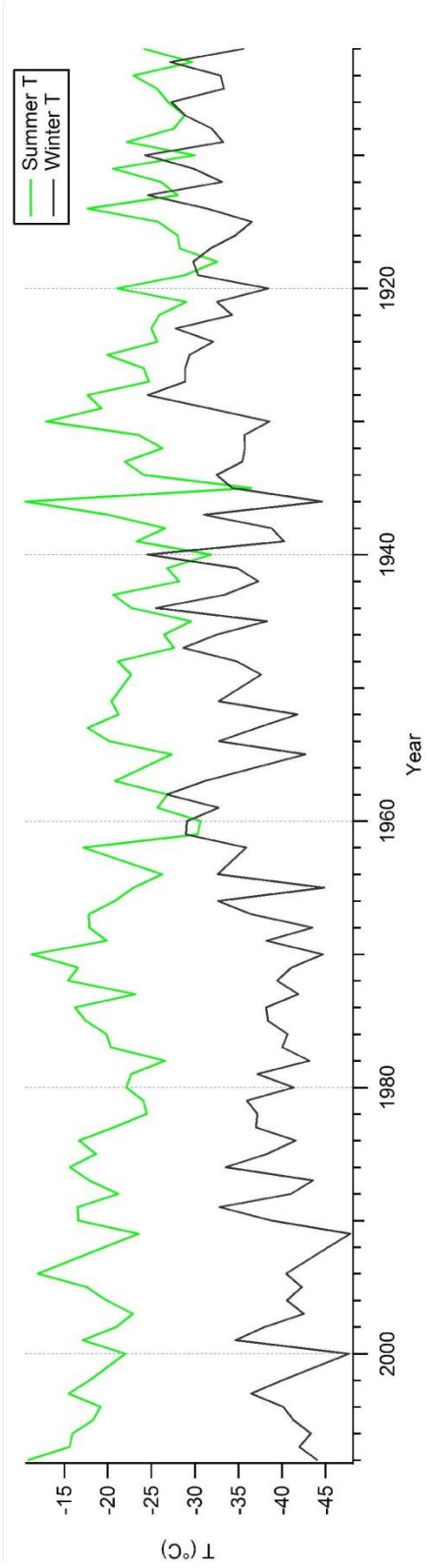

Figure 5-8: The seasonal temperature profile using only the heaviest values as summer and lightest as winters. The difference between trends for summer (green) and winter (blue) can be seen along with the increasing difference after 1960. The gradual temperature change appears to begin after 1980. The trend for the average summer and winter temperature is 0.2°C and -0.15°C per year, respectively, from 1980 to 2007.

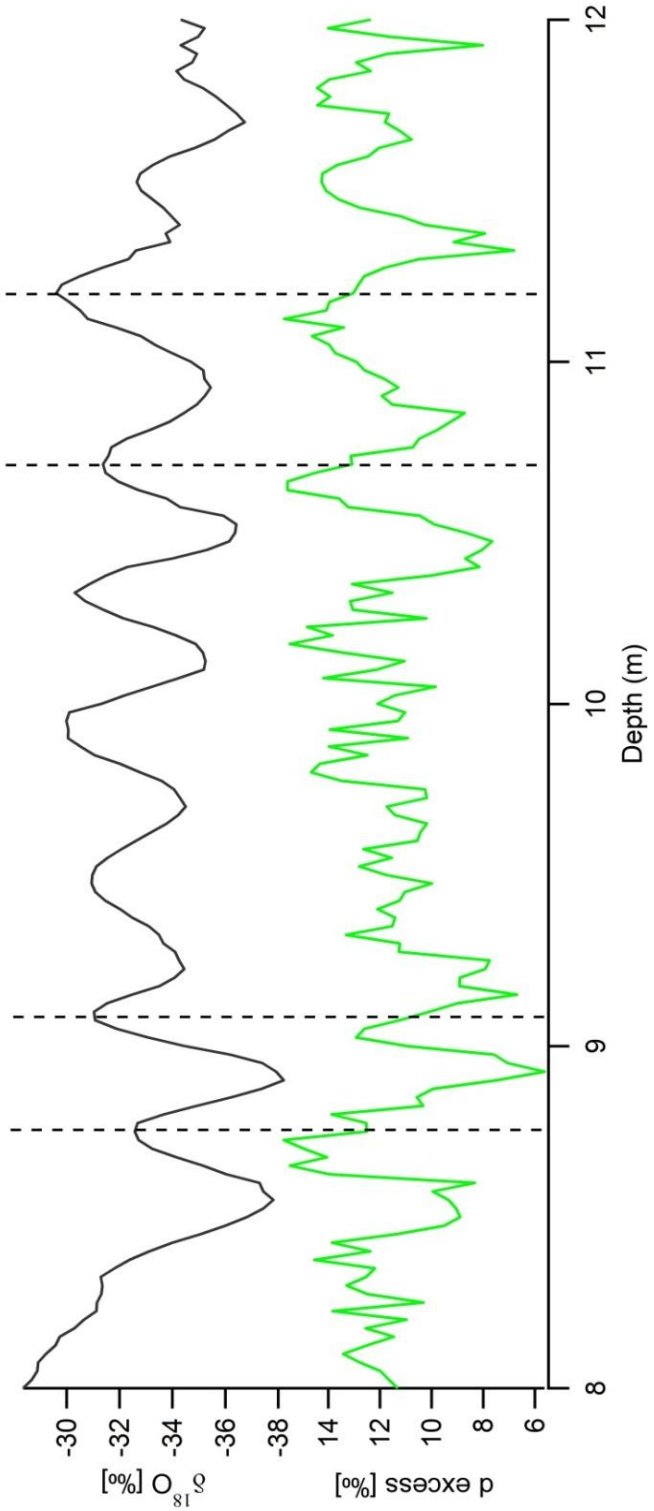

Figure 5-9: A comparison between the d excess (green) and the $\delta^{18}O$ (black) profiles. The difference in the seasonal signal between profiles displays a lag of 2-3 months.

5.5 Natural variability: The comparison between NEEMS308 & NEEMS208.

Although the shallow cores will be analyzed together in another study, it is relevant here to compare two cores, S2 and S3, and observe the natural variations occurring at the NEEM site. The distance between shallow cores is only few meters. In figure 5.10 the annual isotopic profiles of S3 and S2 is compared. The S3 core begins from depths of 0.850 - 0.875m instead of 0-0.025m as S2 does.

In the figure, it can be seen that the cores correlate quite well. Most of the major fluctuations are displayed at the same time in the cores. The small variations that differ between cores are usually of natural origin although sampling and measurements can differ. The years between 1910 and 1914 seem to disagree. S3 documents low $\delta^{18}O$ values while S2 documents high values.

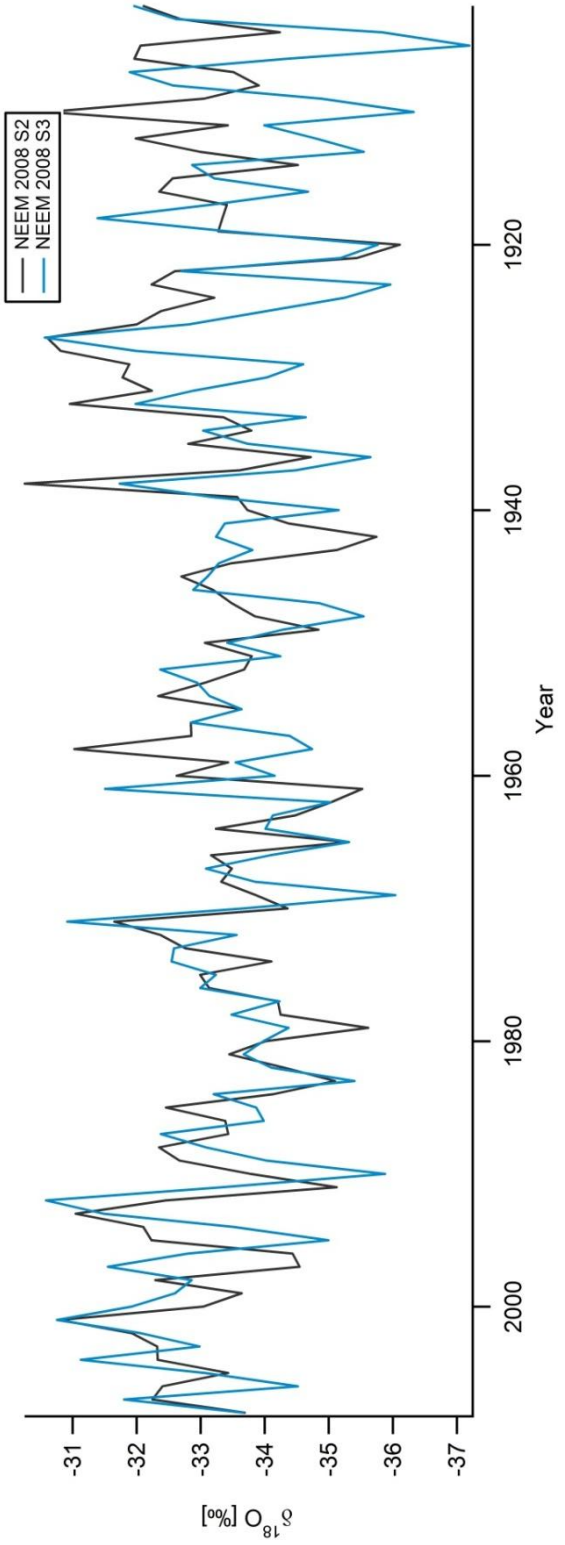

Figure 5-10: A comparison between the NEEM08S2 and NEEM08S3 shallow core. The good correlation is quite visible between S3 (blue) and S2 (black) although there are differences, f. Ex. Between 1910 and 1914.

5.6 Summary and discussions

$\delta^{18}O$ and δD profiles, both raw and deconvoluted, display interesting features. However, the information stored in there is more accessible, particularly when looking at short periods like decades or centuries, when annual and seasonal profiles have been retrieved. As can be seen in the d excess profile in figure 5.2 not much seems to be changing at the moisture source as expected. On a millennial scale the story is different. Then the profile shows distinct oscillations between glacial and interglacial periods, indicating a difference in moisture source (Johnsen et al., 1989).

The temperature rise seen in both annual and summer profiles is consistent with observed recent global warming. Figure 5.11 shows the global mean annual temperature along with the 5 year running mean. According to the figure, significant rise in temperature occurs around 1980. The same is observed in the annual temperature profile of the NEEM08S2 shallow core (fig. 5.7).

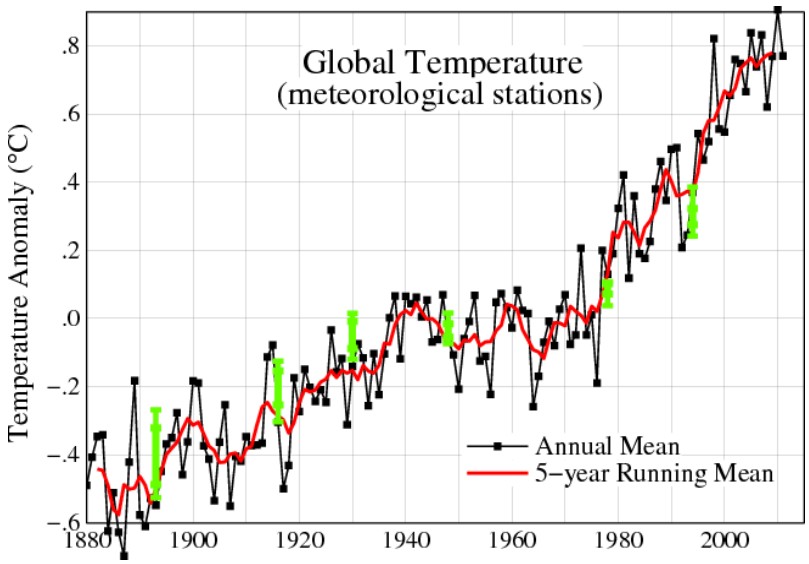

Figure 5-11: Annual global mean temperature anomaly. The green bars represent uncertainty estimations. (Hansen et al., 2001).

The seemingly repeated cycles, visible both in the annual and seasonal profiles (fig. 5.7 and 5.8), could be of several reasons. Here only one is mentioned. Known decadal cycles of natural origin are f. ex. the 22 year solar magnetic cycle. That is the average time it takes for the Sun´s polarity to go one cycle. The 11 year sunspot cycle, more frequently mentioned, is just one-half of that. Recent studies have shown correlation between the 22 year cycle and the atmospheric temperature in mid- northern and mid-southern latitudes (Qu et al., 2012). In a paper by Miyahara et al, (2008) it is also stated that the temperature variations over the 22 year solar cycle seems to be more significant than the 11 year cycle. In fig. 5.12 the mean annual $\delta^{18}O$ value is compared to the total solar irradiation (TSI) for the same period. There, a connection is visible (the dotted lines for reference) where the cold years of 1920, 1944, 1962 occur when the Sun´s irradiation is almost at its lowest. An exception is the cool year of 1981, occurring when the Sun´s irradiation is at its maximum. The irradiation is on average at its minimum every 11 years but that is not seen in the

isotopic signal. Further studies would thus be necessary in order to confirm if the seemingly 22 year cycle visible in the mean annual signal really represents the Sun´s cycle.

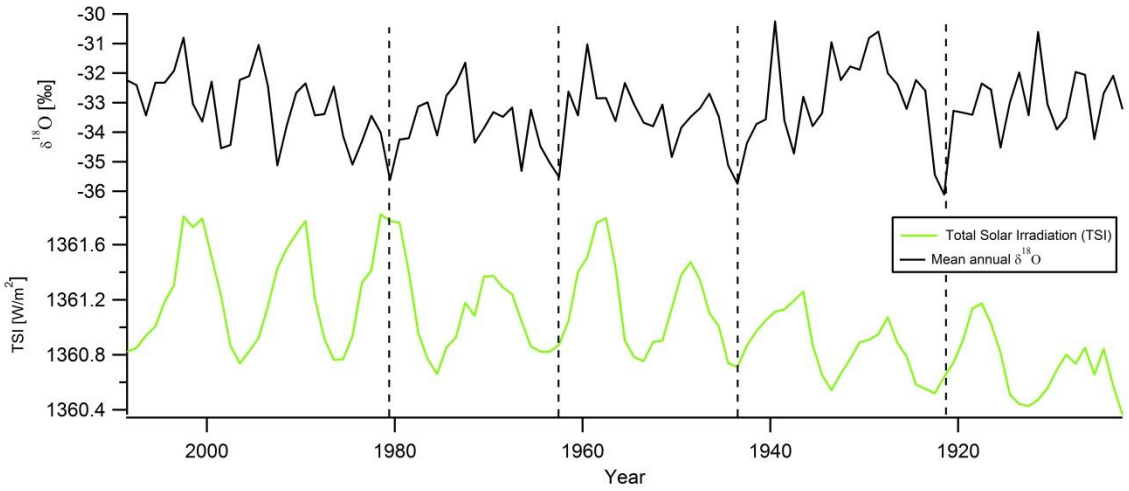

Figure 5-12: Total solar irradiation (Green) (Laboratory for Atmospheric and Space Physics, 2013) compared to the mean annual $\delta^{18}O$ signal (black). The dotted lines are given to facilitate a comparison between the two records.

The 20 year cycle in the isotopic profile appears to be less clear after 1980, coinciding with the time when the global atmospheric temperature rise begins.

The unexpected trend observed in the winter temperature profile (fig. 5.9) may not be that unusual. The profile seems to be slowly heading towards cooler winters after the mid 20th century. In a recent paper by (Petoukhov & Semenov, 2010) it was implied, by using a general circulation model, that the reduced Barents-Kara Sea (in the Arctic area) ice caused reduced continental winter temperatures. That seemingly supplements global warming. They showed that the reduced sea ice resulted in strong anti-cyclonic anomaly over the Polar Ocean along with anomalous easterly advection over the northern continent. If the results of fig. 5.8 will be confirmed by more precise studies, the subject of seasonal changes in a warming world demands further attention.

6 Comparison between the isotopic signal of NEEM S2 2008 shallow core and climatic parameters

A comparison between different climatic parameters and the isotopic profile of NEEM08S2 is presented and interpreted in this chapter. The following climatic parameters are studied:

- North Atlantic Oscillation (NAO)
- Stykkishólmur (Iceland) temperature
- Illulisat (Greenland) temperature
- Baffin Bay Sea Ice Area (BBSIA).

Both linear regression (LR) and multivariable linear regression (MLR) analysis were done in order to estimate the correlation between these parameters and the isotopic signal of NEEM08S2. The calculated correlation coefficient R tells if there is a correlation or not. LR calculations were done using Excel and MLR calculations by using MATLAB. According to Pearson´s Product-Momentum correlation coefficient, correlation estimated from R is of the following:

Table 6-1: Estimate on correlation based on R.

Range:	Correlation
0.0-0.09	None
0.1-0.3	Small
0.3-0.5	Medium
0.5-1.0	High

The same accounts if negative values results from the analysis. Negative values refer to the negative slope resulting when *Y* values decrease while *X* increases. An attempt to estimate the Baffin Bay sea ice area prior to measurements was done. Both data for the Baffin Bay Sea Ice Area and the Baffin Bay Sea Ice Extent exists from the year 1979. The sea ice area represent a fraction of the ocean covered in sea ice (only sea ice) but the sea ice extent represent the areal sum of sea ice (open ocean and sea ice). In the present study, the data for the sea ice area was used. An attempt to estimate the Baffin Bay sea ice area prior to measurements was also done.

6.1 Iceland and climatic parameters

In this part, Stykkishólmur temperature (T) was compared to mean annual NAO index, mean annual $\delta^{18}O$ profile of NEEM08S2, Illulisat T and BBSIA by LR analysis. The results in this part all represent the time period between 1902 and 2007 except BBSIA where data only exists from 1979.

6.1.1 Results

Although NAO is defined by the pressure difference between Iceland and the Azores, small correlation exists between annual Stykkishólmur T and annual NAO index. Analysis between Stykkishólmur annual T and annual NAO gave R= -0.19. 19% of Stykkishólmur T variance can thus be explained by NAO. Analysis between NEEM08S2 $\delta^{18}O$ and Stykkishólmur mean annual temperature resulted in a correlation coefficient value of R = 0.14. That is, 14% of the variance of the NEEM08S2 $\delta^{18}O$ can be correlated to Stykkishólmur T. When annual Stykkishólmur T was regressed with annual Illulisat T it resulted in R = 0.25. Compared to the other parameters, it is interesting to see how well (R = -0.42) Stykkirhólmur T correlates with BBSIA. The correlation coefficients are summarized in table 6.2.

Table 6-2: The Correlation (R) between Stykkishólmur T and NAO, annual $\delta^{18}O$ and Illulisat T.

	Mean annual $\delta^{18}O$	Mean annual NAO index	Illulisat T (°C)	BBSIA (km^2)
Stykkish. T (°C)	0.14	-0.19	0.25	-0.42

6.2 Greenland and climatic parameters

Several climatic parameters from Greenland were studied and analyzed using LR. They are BBSIA, annual NAO index, Illulisat T and the NEEM08S2 mean annual $\delta^{18}O$ profile.

6.2.1 Results

Isotopic profiles from South and mid-Greenland ice cores correlate well with the NAO index (Vinther et al., 2010). That comes as no surprise since this area is defined as one of the influence areas of the NAO, especially South Greenland. Up north, where the NEEM site is located, a different story seems to be recorded in the ice. When annual isotopic and NAO signal are correlated, it results in R = -0.08. Thus no relation appears to be between these two parameters. The analysis between NEEM08S2 $\delta^{18}O$ to BBSIA and Illulisat T resulted in R=-0.28 and R=-0.05 respectively. However, when BBSIA is correlated with Illulisat and NAO, R computes to -0.66 and -0.42 respectively while Illulisat and NAO show small correlation (R=-0.1). The results are summarized in table 6.3.

Table 6-3: Correlation (R) between several different climatic parameters over specified time intervals given in parentheses.

	Annual NAO index	BBSIA (km^2)	Illulisat T (°C)
Annual $\delta^{18}O$	(1902-2007) -0.08	(1979-2007) -0.28	(1902-2007) -0.05
Illulisat T (°C)	(1902-2007) -0.1	(1979-2007) -0.66	
BBSIA	(1979-2007) -0.42		

3.5. Baffin Bay Sea Ice reconstruction

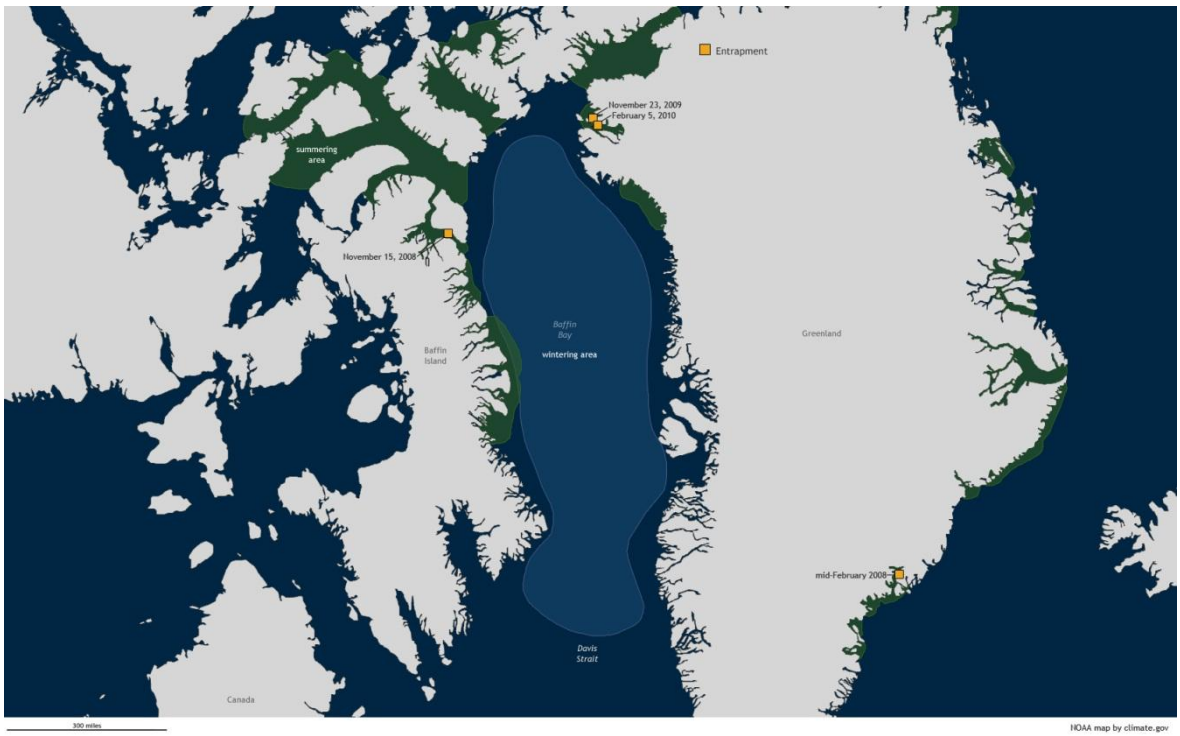

Figure 6-1: Geographic location of the Baffin Bay.

From table 6.3, an interesting pattern emerges. It seems as if $\delta^{18}O$ does not record much of the climatic signal in the area, even though small correlation is detected with BBSIA. However, many things can influence an ice core $\delta^{18}O$ apart from temperature, f. ex. precipitation (or lack if it) and wind. It thus reflects nature better when several different (independent) parameters are used to regress with a dataset of interest. MLR analysis is used in that case. Steen-Larsen et al. (2011) found by using Illulisat T, NAO and the North Atlantic Winter Sea Surface Anomaly (NAWSSA), 58% (R = -0.58) of the variance of the isotopic signal in the shallow NEEM07S3 core between 1979-2004 could be explained. It is thus of interest to see if MLR analysis result in similar signal in the NEEM08S2 shallow core.

6.2.2 Results

To demonstrate the importance of MLR analysis, the BBSIA was first recreated by only using NEEMS208 $\delta^{18}O$ data. The resulting BBSIA was then plotted with the measured profile in fig. 6.2. The resemblance between profiles can hardly be seen (R = 0.06) and thus it is not satisfying to use only the NEEMS208 $\delta^{18}O$ data.

Illulisat T and the NEEM08S2 $\delta^{18}O$ regressed with BBSIA during 1979-2007 result in a very high correlation (R = 0.85) compared to when individual parameters are used (see table 6.3). The constants from the MLR analysis were then used to calculate the BBSIA from 1979-2007. When the resulting calculated BBSIA is plotted along with the measured BBSIA data covering the same period, the correlation between these two profiles is manifested (fig. 6.3). This strong correlation allows for the use of constants from the MLR analysis to recreate the sea ice prior to instrumental measurements (1979). The results are presented in fig. 6.4.

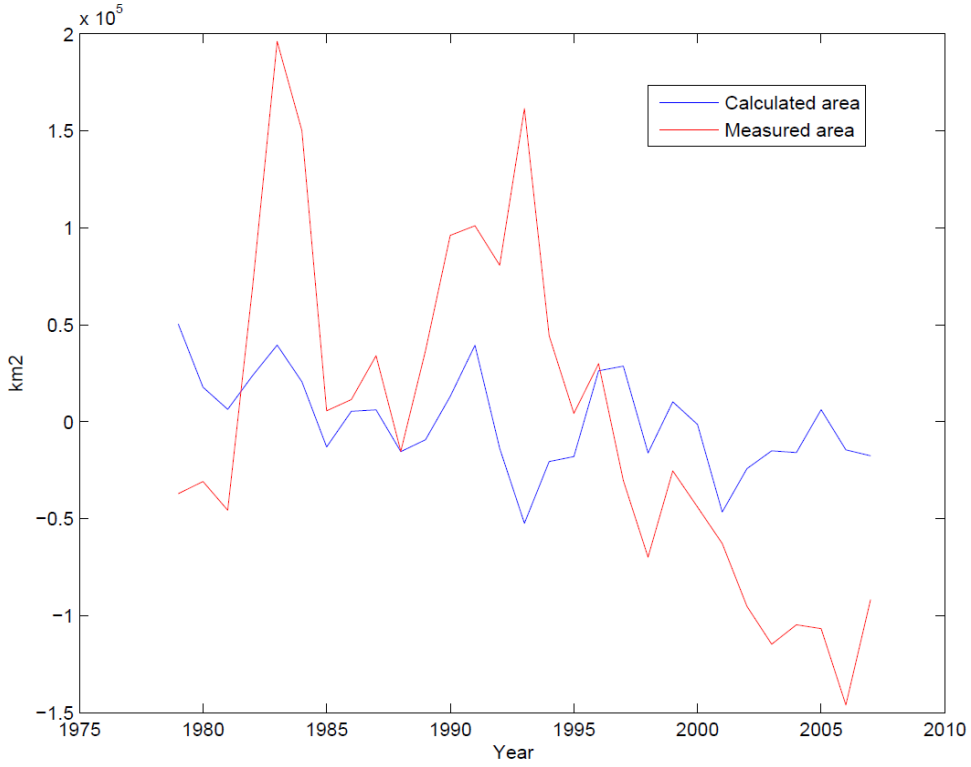

Figure 6-2: The correlation if only $\delta^{18}O$ is used to reconstruct the BBSIA is R = 0.06.

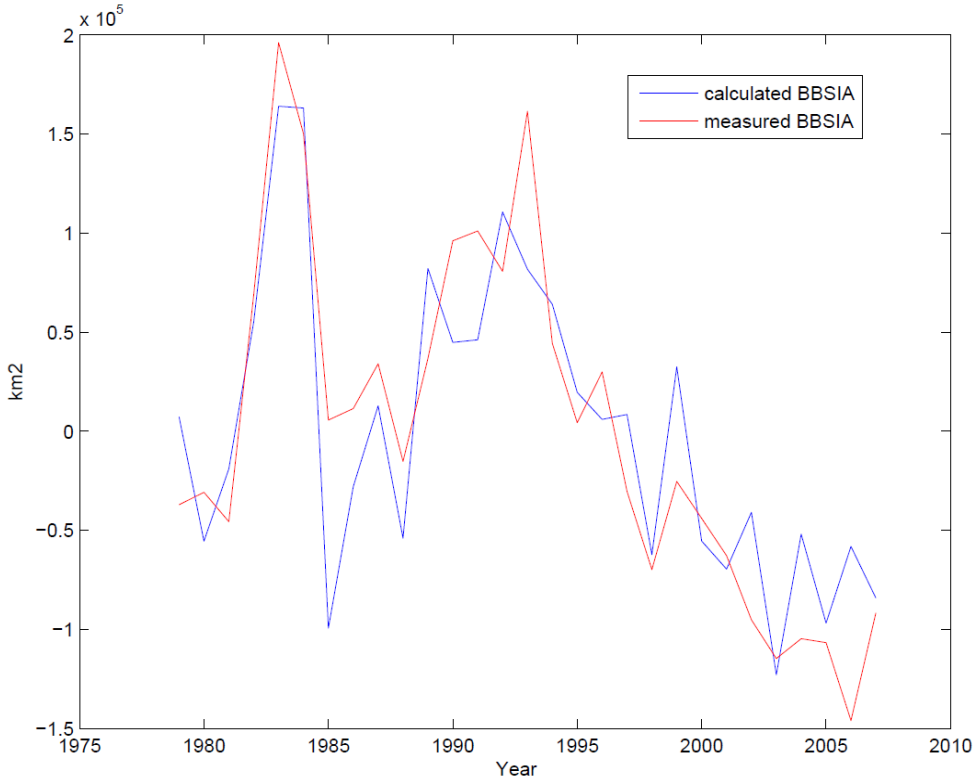

Figure 6-3: Measured (red) and calculated (blue) BBSIA profiles from 1979 to 2007

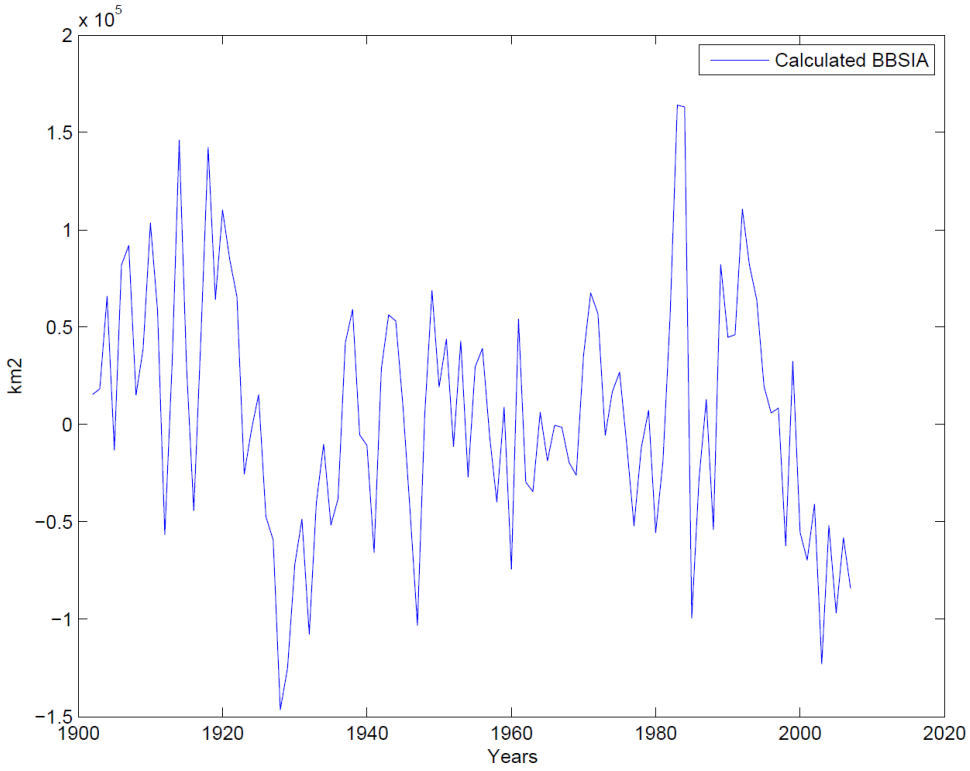

Figure 6-4: Calculated BBSIA from 1902 to 2007.

6.3 Summary and discussions

The low correlation between Stykkishólmur T and the climatic parameters from NW-Greenland should not come as a surprise given the distance between locations. When Stykkishólmur T and the NAO index were compared one might assume a relationship given the definition of the NAO. That was not the case as seen from table 6.2, confirming the results of Björnsson & Jónsson, (2004), who found however a correlation between precipitation in Mývatn, Iceland, and NAO.

The small NAO signal recorded in the NEEM08S2 shallow core is consistent with the signal recorded in the NEEM07S3 (Steen-Larsen et al., 2011). There NAO winter anomaly were correlated with both annual and winter NEEMS307 $\delta^{18}O$, resulting in R = 0.02 and R = -0,01 respectively. Despite that, correlation was detected between the NEEM08S2 $\delta^{18}O$ values and BBSIE (R = -0.34). That is a little higher than the signal recorded in the NEEM08S2 shallow core. The difference could be explained by natural variations between the NEEM shallow cores but further studies are needed.

Stykkishólmur T has frequently been used in climate studies because of the long, ongoing, continuous measurements. The strong correlation between Ammasilak, Greenland (east coast), and Stykkishólmur T (Vinthers et al., 2010) makes the latter one a good representation on temperature for E-Greenland. That could serve as an important link in understanding the relationship between the East and West Greenland. Such understanding could also play a role in explaining the difference observed in ice cores drilled in the south compared to the north.

The reconstruction of the BBSIA for the 20th century reveals some interesting known features. The warm Arctic period between 1920 and 1960 is observed, specially the warm decades of 1930´s and 1940´s. Before 1920, the sea ice area had its maximum peak around 1917-18. 1918 is known as the Great frosty winter in Iceland where sea ice from the North Sea was quite extensive. In a paper by Mysak et al., (1990) the areal sea-ice extent in the Greenland Sea and Baffin Bay/Labrador Sea is estimated by using cross-correlation and complex empirical orthogonal function analyzes. Their results observed for Baffin Bay/Labrador Sea in the years 1972 and 1984 fits well with the ~1970 and ~1980 peaks in fig. 6.4. Similar signal is observed in the NEEM07S3 shallow core, both in the $\delta^{18}O$ values and the BBSIE in the years 1982-84. Also, when looking at fig. 5.6 the same trend is observed at the same time in the annual isotopic signal of NEEM08S2. It is tempting to link this signal observed in NEEM S2, S3 and the BBSIA to the El Chicon eruption in 1982. In that eruption millions of tons of sulfur dioxide was ejected into the stratosphere and encircled the Earth in just few weeks. That caused warming of most of the NH (Robock, 2002). There were exceptions though and they were Alaska, Greenland, the Middle East and China. There the winter of 1982-83 was unusually cold (Robock, 2002). In fig. 6.3, the sea ice area then peaks around 1990´s where melting seems to increase gradually to this present state. That cooling is not as clear in the Stykkishólmur T as in the BBSIA or the Illulisat T.

From the above, it can be estimated that the constructed sea ice presented in fig. 6.3 do represent real natural changes also observed elsewhere in the NH. In fig. 6.5, the profiles of the analyzed parameters are compared. Major climatic events regarding temperature and sea ice anomaly can be observed in the NEEM08S2 $\delta^{18}O$ profile but the link between temperature and BBSIA is more obvious. The correlation between BBSIA and Stykkishólmur T is also interesting. When Stykkishólmur T profile is compared to Illulisat T in fig. 6.5, it can be observed that the trend in both profiles follow each other quite well despite the small correlation between them (table 6.2). Still, there are events, such as the early 80´s that differ between the profiles.

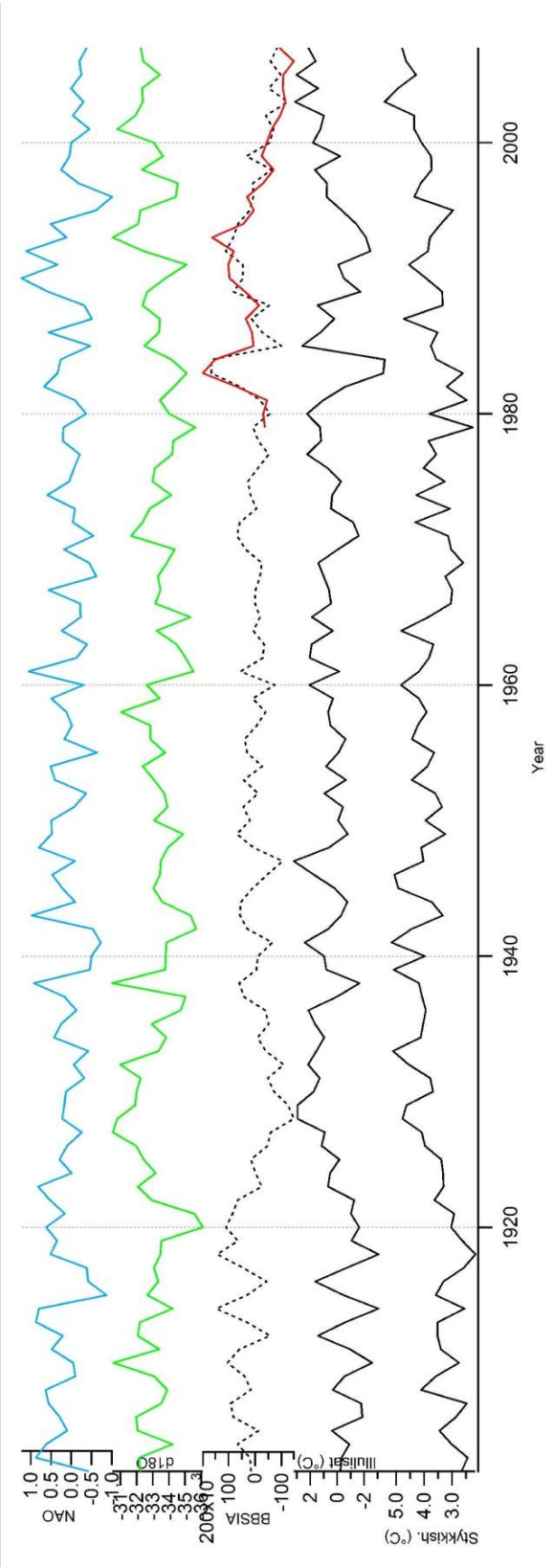

Figure 6-5: Comparison of the climatic parameters studied in chapter 6. They are Stykkishólmur and Illulisat T (°C) (black), reconstructed BBSIA (km^2) for the 20th century (dashed) along with the measured profile (red), the annual $\delta^{18}O$ profile (green) and the annual NAO index (blue).

7 Discussions

During the time-interval of this study, much has changed the course of events. The measurements were a great part of this project so not much time was left for interpretations. When choosing a research questions, the possibilities seemed endless. Many interesting ideas came up along the way, including the effect of large eruption on NH climate and the effect of the Sun on climate for the past centuries. These ideas are beyond the scope of this research project so smaller, more relevant questions were chosen instead, focusing more on regional changes. The Baffin Bay sea ice reconstruction was ideal in the way that similar study had been done by Steen-Larsen et al. (2011) also with a NEEM shallow core (NEEM07S1) but for a shorter period. When the comparison and study between the NEEM shallow cores is done it will result in more accurate data and hopefully shed some new light on the climate changes for the past centuries.

Many questions are left unanswered and many more arose during this study. Much could also have been done differently. These are things I would like to address when reaching the end, both concerning the measurements and the results obtained from them.

First, the use of two different instruments and three different methods to prepare and measure the samples (as described in chapter 4) can result in obvious discrepancies, despite the similar instrumental precision. The Gas Bench was mainly used as an inlet into the IRMS, measuring the NEEM08S2 shallow core samples. It does not allow for simultaneous δD and $\delta^{18}O$ measurements in the IRMS, as previously mentioned, so two runs for the same samples are required. As explained in chapter 4, both the sample preparation and the instrumental protocol for D and ^{18}O are different and time-dependent. Although rare, there were times when it was impossible to start a measurement at the ideal time, thus affecting the results.

There were couple of measurements done by using the TC/EA that measured both δD and $\delta^{18}O$ but given the instrumental problems experienced, the TC/EA was not used except for a few times. The Picarro, introduced late in the process, measures both δD and $\delta^{18}O$ simultaneously with high accuracy and less time. The error is thus different between instruments. Also, a longer refinement time with the Picarro would have been beneficial.

If the measurements were to be repeated, one instrument should be chosen in order to have all the samples calibrated the same and for them to have the same error estimation.

Secondly, how reliable is the isotopic temperature profile? That is a valid question given all the climatic factors and processes influencing a water parcel from the site of evaporation until deposition. To allow for temperature to be reconstructed by using stable water isotopes in ice cores, certain assumptions needs to be followed. At present, the spatial isotope/surface temperature relationship is defined as $\delta = aT_s + b$ for a given region where the slope is $a = d\delta/dT_s$. That relationship (between the spatial and temporal slope) is generally assumed to hold in time throughout that region (Jouzel et al., 1997). Empirical estimation between these two slopes, done by Jouzel et al. (1997), resulted in a lower temporal slope compared to present day spatial slope. Several reasons can be behind this

change, such as changes in the moisture source or changes in precipitation seasonality (Jouzel et al., 1997). Since these changes can vary from one time to another, the timescale of interest needs to be considered before accurate temperature reconstructions can be made. In a paper by Jouzel from 1999, the borehole thermometry and the $\delta^{18}O$ data at the Summit site was compared between the last glacial maximum and present day. The results were that the temperature given by the borehole was -23±2 Kelvin, or twice as large as the temperature from the $\delta^{18}O$ data. This was then confirmed by Werner et al. (2000) using the Hamburg Atmospheric General Circulation Model (ECHAM-4).

One should not expect such discrepancies at shallow depths but this does demonstrate part of the complications when it comes to calibrating the isotopic thermometer. In 2011, the borehole temperature was measured in the main hole. Further studies on borehole temperature and temperature derived from $\delta^{18}O$ data at the NEEM site should reveal the relationship there between.

Thirdly, the seasonal and annual signal depends on the accumulation of precipitation in a given location. If accumulation varies between years it can result in a false trend in the seasonal signal. In order to get a precise seasonal profile, a comparison on the stability of the annual signal between the NEEM shallow cores could have been done. That could be obtained for example by using Maximum Entropy Method (NGRIPmembers) power estimation analysis.

Many things can influence the precipitation as stated before, both known and unknown processes, and with time more and more accurate calibrations can be made. It would have been ideal if temperature measurements had been done at the NEEM site for several decades so a direct comparison between measured and calculated temperature could be done in order to estimate the temporal slope. The comparison and combined studies of the shallow cores from the NEEM site could shed some light on this difference and if it is relevant at this depth.

When studying the annual profile, inter decadal variations seems to be occurring with a period of ~20 years. In chapter 5 it was mentioned in relation to the Solar Magnetic cycle, repeating every 22 years. In order to confirm these oscillations, and to further study it in relation to the Solar Cycle, Fourier analysis on the $\delta^{18}O$ profile would have been ideal in order to increase the signal amplitude. In the paper by Mysak et al. (1990) the existence of an interdecadal cycle was proposed which involved atmospheric, hydrospheric and cryospheric variations in the Arctic. When smooth time series were made of monthly anomalies of sea ice extent in the western Arctic this cycle emerged, also of approximately 20 years. It could thus be interesting to look at the reconstructed sea ice area profile presented in chapter 6 the same way to see if the same pattern occurs. Figure 5.12 shows that these mean annual cycles could be originated from the Sun´s 22 year cycle but is by no means sufficient.

8 Conclusions

1585 samples were measured from the NEEM 2008 S2 shallow core from North West Greenland. That resulted in the following isotopic profiles which were presented and analyzed on a depth scale of 39.6 m:

- $\delta^{18}O$
- δD
- d excess

With the use of the deconvoluted $\delta^{18}O$ profile, the ECM and the d excess an age scale was constructed to the year 1902. Given the temperature dependency of ^{18}O isotopes, the temperature scale was calculated by using Johnsen´s equation from 1989. The annual and seasonal isotopic temperature signal for most of the 20^{th} century was thus presented showing significant rise in local annual temperature after 1980, consistent with other climate data.

Regarding the seasonal temperature, an interesting pattern emerged. It has been a fairly known fact that the annual temperature has been rising for the past decades. However, when looking at the seasonal temperature, the reason for that rise seems to lie mainly in the increasing summer temperature while the winter temperature is getting slightly lower, a trend not well known at present. More detailed studies are needed to confirm this result.

Strong evidence of inter decadal features was found in the annual and seasonal isotopic profiles, also known from previous studies in the area. The Solar magnetic cycle was pointed out as a possible explanation but as with the seasonal and annual signal, it too needs further studies to be confirmed.

Finally, the sea ice area of Baffin Bay was correlated with both $\delta^{18}O$ and Illulisat temperature. The result from the analysis gave rise to the construction of the Baffin Bay sea ice area prior to measurements, or back to the year 1902. That could be of use in the study of the present and future evolution of the Arctic area, a subject of growing importance in a warming world.

References:

Ahrens, C. (Steig et al.). (2009). *Meteorology Today: An Introduction to Weather, Climate and the Environment* (Ninth Edition ed.): Brooks/Cole CENGAGE Learning.

Andersen, K. K., & al., e. (2006). The Greenland Ice Core Chronology 2005, 15-42 ka. Part 1: constructing the time scale. *Quaternary Science Reviews, 25*, 3246-3257.

Appenzeller, C., Stocker, T., & Anklin, M. (1998). North Atlantic Oscillation dynamics recorded in Greenland ice cores. *Science, 282*(5388), 446-449.

Árnason, B. (1976). *Groundwater systems in Iceland traced by Deuterium.* PhD, University of Iceland, Reykjavík.

Bjerknes, J. (1969). Atmospheric teleconnections from the equatorial pacific 1. *Monthly Weather Review, 97*(3), 163-172.

Björnsson, H., & Jónsson, T. (2004). Climate and climatic variability at Lake Myvatn. *Aquatic Ecology, 38*(2), 129-144.

Broccoli, A. J., Dahl, K. A., & Stouffer, R. J. (2006). Response of the ITCZ to Northern Hemisphere cooling. *Geophysical Research Letters, 33*(1), L01702.

Brönnimann, S., Xoplaki, E., Casty, C., Pauling, A., & Luterbacher, J. (2007). ENSO influence on Europe during the last centuries. *Climate Dynamics, 28*(2-3), 181-197. doi: 10.1007/s00382-006-0175-z

Cappa, C. D., Hendricks, M. B., DePaolo, D. J., & Cohen, R. C. (2003). Isotopic fractionation of water during evaporation. *Journal of Geophysical Research, 108*(D16), 4525.

Center for Ice and Climate, (2006). Retrieved from http://www.iceandclimate.nbi.ku.dk/data/

Craig, H. (1961). Isotopic variations in meteoric waters. *Science (New York, NY), 133*(3465), 1702.

Crowley, T. J. (1992). North Atlantic deep water cools the southern hemisphere. *Paleoceanography, 7*(4), 489-497.

Dahl-Jensen, D., Gundestrup, N., Gogineni, S., & Miller, H. (2003). Basal melt at NorthGRIP modeled from borehole, ice-core and radio-echo sound observations. *Annals of Glaciology, 37*(1), 207-212.

Dansgaard, W. (1953). The Abundance of O^{18} in Atmospheric Water and Water Vapour. *Tellus, V*(4).

Dansgaard, W. (1964). Stable isotopes in precipitation. *Tellus, 16*(4), 436-468. doi: 10.1111/j.2153-3490.1964.tb00181.x

Dansgaard, W., Johnsen, S., Clausen, H., Dahl-Jensen, D., Gundestrup, N., Hammer, C., . . . Jouzel, J. (1993). Evidence for general instability of past climate from a 250-kyr ice-core record. *Nature, 364*(6434), 218-220.

Dansgaard, W., Johnsen, S., Clausen, H., & Gundestrup, N. (1973). *Stable isotope glaciology* (Vol. 197): CA Reitzel.

Dansgaard, W., Johnsen, S., Møller, J., & Langway Jr, C. (1969). One thousand centuries of climatic record from Camp Century on the Greenland ice sheet. *Science (New York, NY), 166*(3903), 377.

Dansgaard, W., Johnsen, S. J., Moller, J., & Langway Jr, C. C. (1969). One thousand centuries of Climatic Record from Camp Century in the Greenland Ice sheet. *Science, 166*(3903), 377-380. doi: 10.1126/science.166.3903.377

Dowdeswell, J., & White, J. (1995). Greenland Ice Core Records and Rapid Climate Change. *Philosophical Transactions: Physical Sciences and Engineering, 352*(1699), 359-371.

Earth System Research Laboratory, G. M. D. (2012). Trends in Atmospheric Carbon Dioxide Retrieved 16. april 2012, from http://www.esrl.noaa.gov/gmd/ccgg/trends/

Exploratorium (2012). Retrieved 09.12.2012, from http://icestories.exploratorium.edu/dispatches/big-ideas/polar-geography/

Hansen, J., & Lacis, A. A. (1990). Sun and dust versus greenhouse gases: an assessment of their relative roles in global climate change. *Nature, 346*.

Hansen, J., Ruedy, R., Sato, M., Imhoff, M., Lawrence, W., Easterling, D., . . . Karl, T. (2001). A closer look at United States and global surface temperature change. *J. Geophys. Res., 106*(D20), 23947-23963. doi: 10.1029/2001jd000354

Hansen, J., Sato, M., Ruedy, R., Lacis, A., & Oinas, V. (2000). Global warming in the twenty-first century: An alternative scenatio. *Proceedings of the National Academy of Science, 97*. doi: 10.1073/pnas. 170278997

Hays, J., Imbrie, J., & Shackleton, N. (1976). Variations in the Earth´s Orbit: Pacemaker of the Ice Ages. *Science, 194*(4270), 1121-1132.

Herron, M. M., & Langway Jr, C. C. (1980). Firn densification: an empirical model. *Journal of Glaciology, 25*, 373-385.

Johnsen, S., Clausen, H., Dansgaard, W., Gundestrup, N., Hammer, C., Andersen, U., . . . Steffensen, J. (1997). The δ18O record along the Greenland Ice Core Project deep ice core and the problem of possible Eemian climatic instability. *Journal of Geophysical Research, 102*(C12), 26397-26326,26410.

Johnsen, S., Dahl-Jensen, D., Gundestrup, N., Steffensen, J., Clausen, H., Miller, H., . . . White, J. (2001). Oxyen isotope and paleotemperature records from six Greenland ice-core stations: Camp Century, Dye-3, GRIP, GISP2, Renland and NorthGRIP. *Journal of Quaternary Science, 16*(4), 299-307.

Johnsen, S., Dansgaard, W., & White, J. (1989). The origin of Arctic precipitation under present and glacial conditions. *Tellus B, 41*(4), 452-468.

Johnsen, S. (1977). Stable isotope homogenization of polar firn and ice. *Isotopes and impurities in snow and ice*, 210-219.

Jouzel, J., et al. (2004). EPICA Dome C Ice Cores Deuterium Data. *IGBP Pages/World Data Center for Paleoclimatology Data Contribution Series # 2004-038.* NOAA/NGDC Paleoclimatology Program, Boulder CO, USA.

Jouzel, J. (1999). Calibrating the isotopic paleothermometer. *Science, 286 (5441), 910-911*.

Jouzel, J., Alley, R. B., Cuffey, K., Dansgaard, W., Grootes, P., Hoffmann, G., . . . Shuman, C. (1997). Validity of the temperature reconstruction from water isotopes in ice cores. *JOURNAL OF GEOPHYSICAL RESEARCH-ALL SERIES-, 102*, 26-26.

Jouzel, J., & Merlivat, L. (1984). Deuterium and oxygen 18 in precipitation: modeling of the isotopic effects during snow formation. *Journal of Geophysical Research, 89*(D7), 11749-11711,11757.

Laboratory for Atmospheric and Space Physics, (2013). Retrieved 20.01.2013 from http://lasp.colorado.edu/sorce/data/tsi_data.htm

Luthi, D., Floch, M., Bereiter, B., Blunier, T., Barnola, J., Siegenthaler, U., . . . Stocker, T. (2008). High-resolution carbon dioxide concentration record 650,000-800,000 years before present. *Nature, 453*(15). doi: 10.1038/nature06949

Merlivat, L., & Jouzel, J. (1979). Global climatic interpretation of the deuterium-oxygen 18 relationship for precipitation. *Journal of Geophysical Research, 84*(C8), 5029-5033.

Miyahara, H., Yokoyama, Y., & Masuda, K. (2008). Possible link between multi-decadal climate cycles and periodic reversals of solar magnetic field polarity. *Earth and Planetary Science Letters, 272*(1), 290-295.

Mysak, L. A., Manak, D. K., & Marsden, R. (1990). Sea-ice anomalies observed in the Greenland and Labrador Seas during 1901–1984 and their relation to an interdecadal Arctic climate cycle. *Climate Dynamics, 5*(2), 111-133.

NGRIP members. (2004). High-resolution record of Northern Hemisphere climate extending into the last interglacial period. *Nature*. doi: 10.1038/nature02805

Oeschger, H., Beer, J., Siegenthaler, U., & Stauffer, B. (1984). Late glacial climate history from ice cores. *Geophysical Monograph, 5*(29).

OSS Foundation (2013). Retrieved 15.01.2013 from http://ossfoundation.us/projects/environment/global-warming/north-atlantic-oscillation-nao/

Petit, J. R., et al. (2001). Vostok Ice Core Data for 420.000 years. *IGBP PAGES/World Data Center for Paleoclimatology Data Contribution Seties #2001-076*. NOAA/NGDC Paleoclimatology Program, Boulder CO, USA.

Petit, J. R., Briat, M., & Royer, A. (1981). Ice age aerosol content from East Antarctic ice core samples and past wind strength. *Nature, 293*(5831), 391-394.

Petoukhov, V., & Semenov, V. A. (2010). A link between reduced Barents-Kara sea ice and cold winter extremes over northern continents. *Journal of Geophysical Research, 115*(D21), D21111.

Picarro (2012). Retrieved 09.12, 2012, from http://www.picarro.com/technology/what_is_crds

Qu, W., Zhao, J., Huang, F., & Deng, S. (2012). Correlation between the 22-year Solar Magnetic Cycle and the 22-year Quasicycle in the Earth's Atmospheric Temperature. *The Astronomical Journal, 144*(1), 6.

Rahmstorf, S. (1996). On the freshwater forcing and transport of the Atlantic thermohaline circulation. *Climate Dynamics, 12*(12), 799-811.

Robock, A. (2000). Volcanic eruptions and climate. *Reviews of Geophysics, 38*(2), 191-219.

Rogers, J. C., Bolzan, J. F., & Pohjola, V. A. (1998). Atmospheric circulation variability associated with shallow-core seasonal isotopic extremes near Summit, Greenland. *Journal of Geophysical Research, 103*(D10), 11205-11211,11219.

Souchez, R. (1997). The buildup of the ice sheet in central Greenland. *Geophysical Research, 102*, 26,317-326,323.

Steen-Larsen, H. C., Masson-Delmotte, V., Sjolte, J., Johnsen, S. J., Vinther, B., Bréon, F.-M., . . . White, J. (2011). Understanding the climatic signal in the water stable isotope record from the NEEM shallow firn/ice cores in northwest Greenland. *Journal of Geophysical Research, 116*(D06108). doi: 10.1029/2010JD014311

Steffensen, J. P., Andersen, K. K., Bigler, M., Clausen, H. B., Dahl-Jensen, D., Fischer, H., . . . Jouzel, J. (2008). High-resolution Greenland ice core data show abrupt climate change happens in few years. *Science, 321*(5889), 680-684.

Steig, E., Brook, E., White, J., Sucher, C., Bender, M., Lehman, S., . . . Clow, G. (1998). Synchronous Climate Changes in Antarctica and the North Atlantic. *Science, 282*(92). doi: 10.1126/science.282.5386.92

Urey, H. (1947). The thermodynamic properties of isotopic substances. *Journal of Chemical Society (London)*, 562-581.

U.S Geological Survey (2013). Retrieved 15.01.2013 from http://pubs.usgs.gov/of/2001/ofr01-257/images/figure1.gif

van Loon, H., & Rogers, J. C. (1978). The seesaw in winter temperatures between Greenland and Northern Europe. Part I: General description. *Monthly Weather Review, 106*(3), 296-310.

Vinther, B. (2006). Greenland and North Atlantic climatic conditions during the Holocen – As seen in high resolution stable isotope data from Greenland ice cores. *Ph.D Thesis.* Center for Ice and Climate, Nils Bohrs institute.

Vinther, B., Hansen, A., & von Storch, H. (2003). A major deviation from the NAO temperature seesaw pattern. *Geophysical Research Letters*. doi: 10.1029

Vinther, B. M., Jones, P., Briffa, K., Clausen, H., Andersen, K., Dahl-Jensen, D., & Johnsen, S. (2010). Climatic signals in multiple highly resolved stable isotope records from Greenland. *Quaternary Science Reviews, 29*(3), 522-538.

Werner, M., Mikolajewicz, U., Heimann, M., & Hoffmann, G. (2000) Borehole versus isotope temperature on Greenland: Seasonality does matter. *Geophysical Research Letters. 27 (5), DOI: 10.1029/1999GL006075.*

White, W. B., & Peterson, R. G. (1996). An Antarctic circumpolar wave in surface pressure, wind, temperature and sea-ice extent. *Nature, 380*(6576), 699-702.

Wikipedia, (2013). Retrieved 15.01.2013 from http://en.wikipedia.org/wiki/File:Ice-core-isotope.png